Check for updates

JGR Atmospheres

RESEARCH ARTICLE
10.1029/2022JD037062

Special Section:
Fire in the Earth System

Using Satellite-Derived Fire Arrival Times for Coupled Wildfire-Air Quality Simulations at Regional Scales of the 2020 California Wildfire Season

W. Lassman[1], J. D. Mirocha[1], R. S. Arthur[1], A. K. Kochanski[2], A. Farguell Caus[2], A. M. Bagley[1], M. Carreras Sospedra[3], D. Dabdub[3], and M. Barbato[4]

[1]Lawrence Livermore National Laboratory, Livermore, CA, USA, [2]San Jose State University, San Jose, CA, USA, [3]University of California, Irvine, CA, USA, [4]University of California, Davis, CA, USA

Key Points:

- SFIRE and Fire Inventory from NCAR, two approaches for modeling wildfire smoke emissions, are compared
- Novel methods of ingesting satellite data allow wildfire behavior simulations at scales useful for air quality studies
- Coupled simulations of wildfire spread and atmospheric transport can accurately characterize wildfire impacts on regional air quality

Supporting Information:

Supporting Information may be found in the online version of this article.

Correspondence to:

J. D. Mirocha,
mirocha2@llnl.gov

Citation:

Lassman, W., Mirocha, J. D., Arthur, R. S., Kochanski, A. K., Farguell Caus, A., Bagley, A. M., et al. (2023). Using satellite-derived fire arrival times for coupled wildfire-air quality simulations at regional scales of the 2020 California wildfire season. *Journal of Geophysical Research: Atmospheres*, *128*, e2022JD037062. https://doi.org/10.1029/2022JD037062

Received 6 MAY 2022
Accepted 16 DEC 2022

Author Contributions:

Conceptualization: W. Lassman, J. D. Mirocha, A. K. Kochanski, M. Barbato
Formal analysis: W. Lassman, J. D. Mirocha, R. S. Arthur, A. K. Kochanski, M. Carreras Sospedra, D. Dabdub, M. Barbato

© 2023. The Authors.
This is an open access article under the terms of the Creative Commons Attribution-NonCommercial-NoDerivs License, which permits use and distribution in any medium, provided the original work is properly cited, the use is non-commercial and no modifications or adaptations are made.

Abstract Wildfire frequency has increased in the Western US over recent decades, driven by climate change and a legacy of forest management practices. Consequently, human structures, health, and life are increasingly at risk due to wildfires. Furthermore, wildfire smoke presents a growing hazard for regional and national air quality. In response, many scientific tools have been developed to study and forecast wildfire behavior, or test interventions that may mitigate risk. In this study, we present a retrospective analysis of 1 month of the 2020 Northern California wildfire season, when many wildfires with varying environments and behavior impacted regional air quality. We simulated this period using a coupled numerical weather prediction model with online atmospheric chemistry, and compare two approaches to representing smoke emissions: an online fire spread model driven by remotely sensed fire arrival times and a biomass burning emissions inventory. First, we quantify the differences in smoke emissions and timing of fire activity, and characterize the subsequent impact on estimates of smoke emissions. Next, we compare the simulated smoke to surface observations and remotely sensed smoke; we find that despite differences in the simulated smoke surface concentrations, the two models achieve similar levels of accuracy. We present a detailed comparison between the performance and relative strengths of both approaches, and discuss potential refinements that could further improve future simulations of wildfire smoke. Finally, we characterize the interactions between smoke and meteorology during this event, and discuss the implications that increases in regional smoke may have on future meteorological conditions.

Plain Language Summary Smoke from wildfire is a growing public health concern. In order to help predict wildfire smoke exposure, we need tools that can accurately forecast where concentrated smoke will go. However, wildfires are difficult to simulate because they change quickly in response to the weather, and the behavior is sensitive to the underlying fuel which is often not well-characterized. We used satellite observations of wildfires to constrain simulations of wildfire spread, allowing us to accurately simulate many fires occurring at the same time. This enabled simulations of 1 month of the 2020 California wildfire season, one of the worst on record. We evaluated the accuracy of this simulation using measurements of surface air quality, and using a similar simulation with a more widely used methodology. The results from this study will help us develop more accurate tools to predict smoke concentrations and impacts on meteorology during future events.

1. Introduction

Wildfires are an important process of the earth-climate system (Liu et al., 2014). In general, fires are a natural process for managing biomass load and biogeochemical fluxes between the biosphere, atmosphere, and soil (Crutzen & Andreae, 1990). Fires also produce smoke that can impact the earth's radiative balance and cloud processes (Bauer et al., 2010; Carter et al., 2020; Ramnarine et al., 2019). Due to connections between hot and dry conditions and fire activity, wildfires are becoming more prevalent and more intense as the earth's climate continues to warm, especially in the Western US (Westerling et al., 2006). The smoke produced from this increasing number of fires can produce hazardous air quality conditions, leading to large detectable increases in population-level mortality and morbidity (Gan et al., 2017; Reid et al., 2016; Yao et al., 2020), even at long distances from wildfires (O'Dell et al., 2021). As climate changes, increases in wildfire smoke emissions may offset many of the air quality benefits yielded from regulation of anthropogenic sources of aerosols through the Clean Air Act (Ford et al., 2018; O'Dell et al., 2019).

Funding acquisition: J. D. Mirocha, M. Barbato
Investigation: W. Lassman, A. M. Bagley
Methodology: A. K. Kochanski, A. Farguell Caus
Project Administration: W. Lassman, J. D. Mirocha
Resources: J. D. Mirocha
Supervision: J. D. Mirocha, R. S. Arthur, A. K. Kochanski
Validation: W. Lassman, A. M. Bagley
Visualization: W. Lassman, A. M. Bagley
Writing – original draft: W. Lassman
Writing – review & editing: J. D. Mirocha, R. S. Arthur, A. K. Kochanski, A. Farguell Caus, A. M. Bagley, M. Carreras Sospedra, D. Dabdub, M. Barbato

Wildfire smoke impacts are multifaceted. Therefore, as wildfire smoke events become more frequent, modeling tools must be developed for many smoke-related applications. These applications include air quality forecasting (Pavlovic et al., 2016; Yang et al., 2011), retrospective health impact assessments (Gan et al., 2017; Lassman et al., 2017; O'Dell et al., 2021), quantification of climate impacts (Hodshire et al., 2019; Ramnarine et al., 2019), among others. While each of these applications requires some understanding of fire emissions and the subsequent atmospheric transport and chemical processing, they also require different levels of fidelity. Studies focused on climate impacts require an average representation of many fires in many different ecosystems and conditions over a long time. Air quality forecasts prioritize lightweight modeling frameworks that can produce fast results to assist in real time response to ongoing fire events, thus sacrificing detailed physics for computing speed. However, higher fidelity may also be required for certain forecast applications. Finally, retrospective case studies of individual fire events can incorporate highly detailed information about the event alongside high-fidelity physical models; these studies often leverage expensive computations, along with an opportunity to optimize simulation input parameters.

The complex dynamics and poorly constrained behavior of many wildfires can complicate the latter approach, which is the focus of the present work. Wildfire behavior that controls smoke emission depends on difficult-to-predict ignition sources, heterogeneity of fuel types and fuel moisture, regional weather, and local microclimate impacted by fire-atmosphere interactions and terrain. Air quality impacts of wildfires depend on the smoke dispersion, which is driven by the atmospheric state and large-scale winds, and on the chemical processes occurring in the atmosphere. Wildfire smoke can absorb or reflect solar radiation, causing significant but challenging-to-recreate effects on local temperatures that in turn feedback on the boundary layer depth, vertical mixing, and local winds (Kochanski et al., 2019). Thus, improving the fidelity of highly detailed wildfire smoke simulations requires attention to many components of the modeling system.

Understanding and modeling wildfire smoke physics and chemistry are active areas of research. Recent observational campaigns and lab studies have advanced the understanding of underlying chemical composition and evolution of wildfire smoke (Barry et al., 2021; Jen et al., 2019; Lindaas et al., 2021; O'Dell et al., 2020). Furthermore, advances in dynamic fire models have made it computationally feasible to link fire spread to chemical emissions inside a coupled atmospheric modeling framework (Kochanski et al., 2015, 2019; Mallia et al., 2018). Due to the complexity of modeling fire spread, and computational requirements these simulation studies have previously been limited in terms of domain size, duration, and number of fires number of fires. However, recent advances in machine learning have allowed the use of remote sensing data to nudge dynamic fire spread models toward observed fire progression history, which can lead to improved spatial and temporal accuracy of fire emissions (Farguell et al., 2021). These advances have enabled wildfire simulations with realistic representations of the many physical and chemical processes impacting fire emission, plume dynamics, and smoke dispersion. Despite these advances, such simulations remain dependent upon other poorly constrained or unknown parameters that add uncertainty to model results.

In contrast to direct simulation of an advancing fire front, there are other approaches to representing wildfires in Chemical Transport Models (CTMs) used for air quality simulations. A standard approach for CTM studies is to use emissions inventories to specify emissions locations and fluxes. Emissions inventories are constructed in a manner that is easy to scale to arbitrary sizes and numbers of source types. Such inventories exist for anthropogenic emissions (e.g., the Environmental Protection Agency National Emissions Inventory) and biogenic sources (e.g., MEGAN). Whereas numerous inventories for biomass burning are available, wildfires are challenging to represent in this manner because they have dynamic behavior and can create feedbacks with underlying atmospheric transport. The Fire Inventory from NCAR (FINN) (Wiedinmyer et al., 2011) is a widely used emissions inventory (Jiang et al., 2012; Val Martin et al., 2013; Wiedinmyer et al., 2006), which can be considered as a "reference method" for the present study. FINN uses satellite-based fire detections and remotely sensed landcover datasets to produce estimates of wildfire emissions in near real time.

In this study, we explore the utility of a coupled wildfire-atmospheric-chemical model at scales necessary for conducting regional air quality studies. We present atmospheric simulations with online fire spread, smoke-atmosphere interaction and feedbacks, and complete chemical emissions from non-wildfire sources, for a month-long segment of a historic fire season: the 2020 Wildfire Season in Northern California. We compare two approaches: (a) a reference method using the Weather Research and Forecasting (WRF) (Skamarock et al., 2008) model with Chemistry (WRF-Chem) (G. A. Grell et al., 2005), with preprocessed anthropogenic

21698996, 2023, 6, Downloaded from https://agupubs.onlinelibrary.wiley.com/doi/10.1029/2022JD037062 by University Of California Irvine Science Library Serials, Wiley Online Library on [29/09/2026]. See the Terms and Conditions (https://onlinelibrary.wiley.com/terms-and-conditions) on Wiley Online Library for rules of use; OA articles are governed by the applicable Creative Commons License

21698996, 2023, 6, Downloaded from https://agupubs.onlinelibrary.wiley.com/doi/10.1029/2022JD037062 by University Of California Irvine Science Library Serials, Wiley Online Library on [29/09/2026]. See the Terms and Conditions (https://onlinelibrary.wiley.com/terms-and-conditions) on Wiley Online Library for rules of use; OA articles are governed by the applicable Creative Commons License

and fire emissions (FINN; Wiedinmyer et al., 2006); and (b) WRF-SFIRE-Chem (Kochanski et al., 2015), with similarly processed anthropogenic emissions but fire emissions and plume rise resolved using SFIRE, a dynamic fire spread model, rendering location and intensity of fire emission and heat fluxes as a function of time. A third simulation, using WRF-Chem with no biomass burning emissions present, provides a "control" simulation. We describe differences in the representations of the fires through inputs to WRF-Chem using these two approaches and compare these representations to remotely sensed fire characteristics. Next, we compare modeled concentrations of particulate matter less than 2.5 μm in diameter ($PM_{2.5}$) to surface measurements, and the model-derived Aerosol Optical Depth (AOD) to remotely sensed quantities. We discuss the practical differences between the two different approaches for representing wildfires in CTMs, and what options exist for model improvement. Finally, we investigate the impact of smoke on surface temperature, and winds.

2. The 2020 California Wildfire Season

The 2020 California wildfire season reported the most area burned in recorded California history, with over 1.5 million hectares of area burned ("Fire Season," 2021). The fire season in Northern California began in earnest in the middle of August, after a series of nighttime thunderstorms that produced an abundance of dry lightning passed through the San Francisco (SF) Bay area. Numerous lightning strikes began a series of fires, which then grew after warm windy conditions returned, producing several wildfire complexes close to the SF Bay Area. The first half of the time period of interest (19–31 August), was dominated by smoke from the numerous wildfire complexes as they grew and merged into larger fires. In the densely populated SF Bay area, air quality in August was highly variable, due to the numerous fires interacting with complex meteorological, orographic and marine circulations in the region.

In the second half of the time period (August 31 to September 15), the smoke was dominated by emissions from larger megafires. The August Complex Fire merged into a single large fire, becoming the largest wildfire in recorded CA history ("August Complex Information - InciWeb the Incident Information System," 2020). In addition to the August Complex Fire, the Creek Fire in the Sierra Nevada mountains was ignited after a lightning strike on 4 September. This notable fire rapidly grew into a large fire that produced a pyrocumulonimbus cloud that reached over 14 km above sea level ("Creek Fire Information - InciWeb the Incident Information System," 2020). Finally, another group of wildfire complexes near Portland, OR, merged to produce a large wildfire that, due to synoptic-scale weather conditions, sent smoke to Northern CA during the second week of September. Northern CA air quality conditions in September were thus dominated by smoke from the above three megafires: initially the August Complex Fire, then the Creek Fire, and finally the Portland complex fires. During the end of the study period, highly complex interactions between regional smoke inundation and a marine layer near the coast produced sharp gradients in surface $PM_{2.5}$. This range of fire sizes and conditions presents a compelling case study for evaluating the performance of the fully coupled WRF-SFIRE-Chem system, as compared to the reference WRF-Chem FINN simulation, across a variety of smoke scenarios.

3. Methods and Data

3.1. Simulation Setup

3.1.1. Base WRF-Chem Setup

To simulate the evolution of smoke in the atmosphere, we use WRF-Chem (G. A. Grell et al., 2005). The WRF framework solves the equations of motion for a fluid on a rotating sphere with moist processes, coupled to radiation, land surface, planetary boundary layer, and cloud microphysics models (Skamarock et al., 2008). Additionally, the inclusion of WRF-Chem enables modules for atmospheric gas and aerosol phase chemistry. A unique ability of WRF-Chem is its online coupling of aerosols with the meteorological microphysics and radiation solvers, allowing aerosol effects on temperature and cloud processes to feedback on the atmospheric state. In the context of wildfires, this capability allows the model to capture smoke shading and the resulting impact on surface heat fluxes and atmospheric stability, as well as fire effects on convection (G. Grell et al., 2011).

In this study, we simulate the period from 14 August 2020 through 15 September 2020, allowing 5 days for simulation spinup before the fire activity began impacting air quality. The WRF configuration used 3 nested domains with horizontal grid spacing of 9 km (D01), 3 km (D02), and 1 km (D03), respectively, as shown in Figure 1a.

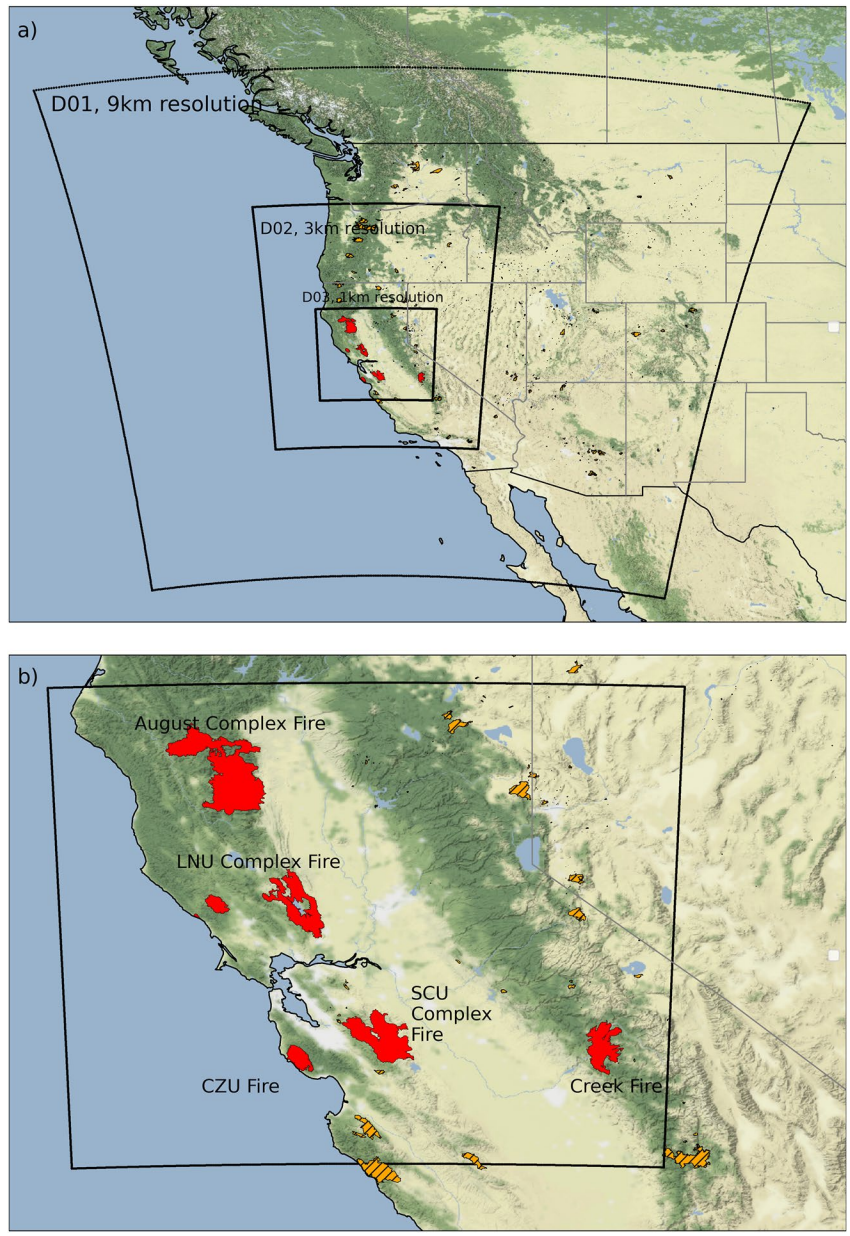


Figure 1. Model domain: (a) map of Weather Research and Forecasting simulation domains, and (b) a close-up of the innermost domain. Burned areas corresponding to the major fires are shaded in red, while a comprehensive (but not exhaustive) data set of other fires are overlaid in orange.

Figure 1b shows a close-up of the innermost domain with the large fire areas from this time period overlaid in red. The model configuration used a vertical coordinate system with 51 vertical levels, based on those of the High Resolution Rapid Refresh (HRRR)-Smoke (Benjamin et al., 2016, 2020), an operational smoke forecasting tool. We used reanalysis from the Global Forecasting System (GFS) ("NCEP GFS 0.25 Degree Global Forecast Grids Historical Archive," 2015) to provide the model with meteorological initial and boundary conditions. Throughout the simulation, the outermost domain is nudged toward the analysis product on an hourly timescale to ensure that the simulation reproduces the large-scale atmospheric state that was present throughout the simulated period. For the WRF model physics, we use the CONtiguous United States (CONUS) physics suite which includes the following: the Thompson microphysics scheme (Thompson et al., 2004), Mellor-Yamada-Jancic planetary boundary layer scheme (Mellor & Yamada, 1982, 2001), NOAH land surface scheme (Campbell et al., 2019), and Rapid Radiative Transfer Model longwave and shortwave radiative transfer schemes (Iacono et al., 2008).

21698996, 2023, 6, Downloaded from https://agupubs.onlinelibrary.wiley.com/doi/10.1029/2022JD037062 by University Of California Irvine Science Library Serials, Wiley Online Library on [29/09/2026]. See the Terms and Conditions (https://onlinelibrary.wiley.com/terms-and-conditions) on Wiley Online Library for rules of use; OA articles are governed by the applicable Creative Commons License

21698996, 2023, 6, Downloaded from https://agupubs.onlinelibrary.wiley.com/doi/10.1029/2022JD037062 by University Of California Irvine Science Library Serials, Wiley Online Library on [29/09/2026]. See the Terms and Conditions (https://onlinelibrary.wiley.com/terms-and-conditions) on Wiley Online Library for rules of use; OA articles are governed by the applicable Creative Commons License

For the chemistry model, we use the Model for Ozone And Related Tracers (MOZART) gas-phase chemical mechanisms with Goddard Chemistry Aerosol Radiation and Transport (GOCART) aerosol scheme, the combination of which is referred to as MOZCART (Emmons et al., 2010; Pfister et al., 2011). Non-fire emissions were obtained and prepared from the National Center for Atmospheric Research (NCAR) WRF-Chem emissions guide (https://www2.acom.ucar.edu/wrf-chem/wrf-chem-tools-community). Readers should refer to this reference for setting up their own WRF-Chem simulations; whereas we will briefly describe the configurations used here. Anthropogenic emissions were represented by the EPA National Emission Inventory 2014 data set (US EPA, 2016) and were interpolated to the WRF-Chem grid using the ANTHRO_EMIS emissions preprocessor available from NCAR. Biogenic emissions were represented using MEGAN (Guenther et al., 2012). Chemical initial and boundary conditions were derived from the Whole Atmosphere Community Climate Model (Gettelman et al., 2019).

For a complete summary of the WRF setup, refer to the namelist files included in Section S1 in Supporting Information S1.

3.1.2. Model Experiment: Different Representations of Wildland Fire

We conduct three separate WRF-Chem simulations that use the base WRF-Chem setup but differ in their representation of the wildfire emissions. The first simulation had no biomass burning emissions present, referred to as NoFire simulation hereinafter. We treat this simulation as a "control" scenario to understand the counterfactual atmospheric state (e.g., $PM_{2.5}$ concentrations, temperature, windspeed) in the absence of fire. Next, we conduct a simulation that used FINNv1.0 (Wiedinmyer et al., 2011), referred to as FINN simulation hereinafter. The FINN simulation can be thought of as a "reference method" for this study. FINN uses Moderate Resolution Imaging Spectroradiometer (MODIS) fire detections to determine active fires in near real time. These fire detections are overlaid on MODIS Landcover Classification data to estimate the type of fuel that is being consumed. The total fire area, and the fuel consumption per unit area, are both assumed functions of landcover type. Because MODIS Fire Detections are available at daily resolution, FINN is a daily product; it provides no information about changes in fire location or intensity throughout a day. Instead, a diurnal cycle based on wildfire climatology (Mu et al., 2011) is applied to fire intensity during the WRF-Chem preprocessing stage which scales the fire heat and chemical emission fluxes. The vertical distribution of smoke is derived from an offline plume rise parameterization (Fretias et al., 2010, 2007), which is based on fire area and heat flux per unit area, as well as on local atmospheric conditions. The fire heat flux is also tied to the diurnal profile. Because FINN does not track fuel consumption, pixels will continue to emit constant emissions (modulated by the imposed diurnal cycle) each day that this pixel has a fire detection associated with it; only when MODIS no longer detects fire at this point will the fire emissions cease.

Finally, we conduct a WRF-Chem simulation where the smoke emissions are coupled to the SFIRE fire spread model, which is referred to as SFIRE simulation hereinafter. SFIRE is an online fire spread model that includes two-way coupling between the fire rate of spread the atmospheric forcing at the same timestep (Andrews, 2013). Instead of an offline plume rise model, the pyroconvection is resolved directly on the model grid since the heat fluxes computed by the fire component are injected into the atmosphere along with the emission fluxes. The fire spread is simulated on a subgrid within domain D03 of our WRF setup, with a subgrid grid cell size ratio of 10; therefore, the wildfire spread model, and fuel consumption, are simulated with 100 m grid spacing. For this study, we use the 30 m Anderson Fuel classification data from LANDFIRE, which is interpolated to the SFIRE fire subgrid using standard WRF preprocessing routines.

In order to constrain the fire progression and limit the impact of the fire rate of spread model on fire emissions, we force the fire spread model with prescribed fire arrival times that are generated from a Support Vector Machine (SVM) algorithm following the methods outlined in Farguell et al. (2021). SVMs are supervised machine-learning algorithms that determines a vector in an n-dimensional phase space that separates points into two categories. In this application, the SVM ingest the MODIS L2 Active Fire data fire product. This data product is available twice daily, and includes classification of surface pixels as "active fire," "no fire," and "no data," along with a parameter quantifying the uncertainty, as input data. Aside from the satellite detection, the algorithm was also trained using National Interagency Fire Center archived perimeters. The final model output is the "fire arrival time," that is, the date and time when a certain pixel in the model domain becomes "on fire," This algorithm allows a WRF-SFIRE simulation to bypass the surface fire spread model built on the Rothermel method, and replay historic fires with a high degree of accuracy, depending on the effectiveness of the SVM for each specific case. Because the SVM

21698996, 2023, 6, Downloaded from https://agupubs.onlinelibrary.wiley.com/doi/10.1029/2022JD037062 by University Of California Irvine Science Library Serials, Wiley Online Library on [29/09/2026]. See the Terms and Conditions (https://onlinelibrary.wiley.com/terms-and-conditions) on Wiley Online Library for rules of use; OA articles are governed by the applicable Creative Commons License

approach requires remotely sensed active fire detections, this approach cannot be used to forecast fire spread during an ongoing incident. This approach allows us to derive fire location estimates for the chemical emissions using an automated algorithm, which leverages satellite-derived fire detections from polar-orbiting MODIS and VIIRS satellite platforms along with airborne fire perimeters. Thus, we are able to conduct SFIRE simulations on a regional-scale model domain with many different fire events, which would have otherwise been intractable. For fires occurring outside of domain D03, we use the FINN emissions inventory to represent emissions, as in the baseline FINN simulation.

3.2. Data Used for Simulation Evaluation

3.2.1. Surface Observations

To evaluate the $PM_{2.5}$ concentrations estimated by the simulations, we use the EPA Air Quality System (AQS) Hourly data product (88101); (US EPA, 2014). This data product is aggregated from measurements made by state and local agencies. This particular network of monitoring sites are regulatory monitors that use Federal Reference Methods or Federal Equivalent Methods to measure surface $PM_{2.5}$ concentrations at hourly temporal resolution. Approximately 50 surface monitor sites were located inside our simulation domain, clustered around urban and suburban areas. Model-derived $PM_{2.5}$ concentrations are interpolated to surface measurement sites using inverse distance weighting.

Surface meteorological observations of temperature and wind speed are obtained from 60 weather stations in the Northern California area. Hourly weather station data is downloaded from MesoWest (Horel et al., 2002). Quality control procedures are applied including removing duplicate time entries and inconsistent temperature and wind measurements. For model validation, the measurements closest to the hour are chosen and the hourly WRF simulation output is bilinearly interpolated to the weather station locations. Model-measurement comparisons were conducted at two Automated Surface Observing Systems sites, but additional Remote Automatic Weather Stations are included in map plots for additional comparisons.

3.2.2. Satellite Observations

To evaluate fire area and intensity inputs to WRF-Chem, we use the GOES Fire Detection and Characterization (FDC) Level 2 product (Schmidt et al., 2013). GOES-17 is a geostationary platform which allows continual observation of our simulation domain; the FDC data product includes fire area and fire radiative power (FRP). These data are available at 15 min increments and at a spatial resolution of approximately 2 km over our study domain. We use this data product to quantify fire growth and activity as a function of time, aggregated across the entire simulation domain.

To analyze the smoke dispersion, we use retrievals of AOD Level 2 10 km data product from the MODIS satellite platforms, in conjunction with the merged Deep Blue/Dark Target data product (Levy et al., 2013). This data product is used to qualitatively compare the spatial extent of smoke plumes obtained from the FINN and SFIRE simulations to remotely sensed observations of smoke.

4. Results and Discussion

4.1. SFIRE Versus FINN Fire Area and Smoke Emissions

We characterize the differences in model inputs to WRF-Chem in terms of emissions area, fluxes, and their spatial and temporal evolution in order to investigate the differences between SFIRE and FINN applied to regional air quality simulations. Figure 2 shows a 24-hr snapshot of the fire area and progression in SFIRE (a, d), the fire area in FINN (b, e), and the corresponding fire detections from GOES-17 satellite observations (c, f), at two snapshots in time. The top row (a–c) depicts 18 August at 0800 UTC, when the fires were mostly scattered wildfire complexes; the bottom row (d–f) shows 7 Septemeber at 1000 UTC, when the fires of interest were the August Complex megafire and Creek Fire. In Figures 2a and 2d (corresponding to the SFIRE simulations), the shaded red shows active fire pixels, where the fuel load variable decreased over the 24-hr period, indicating that this pixel was "on fire" in SFIRE and emitting smoke species. For SFIRE, the initial fuel load is a predetermined quantity that is a function of fuel category (Albini, 1976). In SFIRE, once a pixel has ignited, it continues to burn until 100% of the initial fuel load is consumed, and the timescale of fuel consumption is determined by a simplified

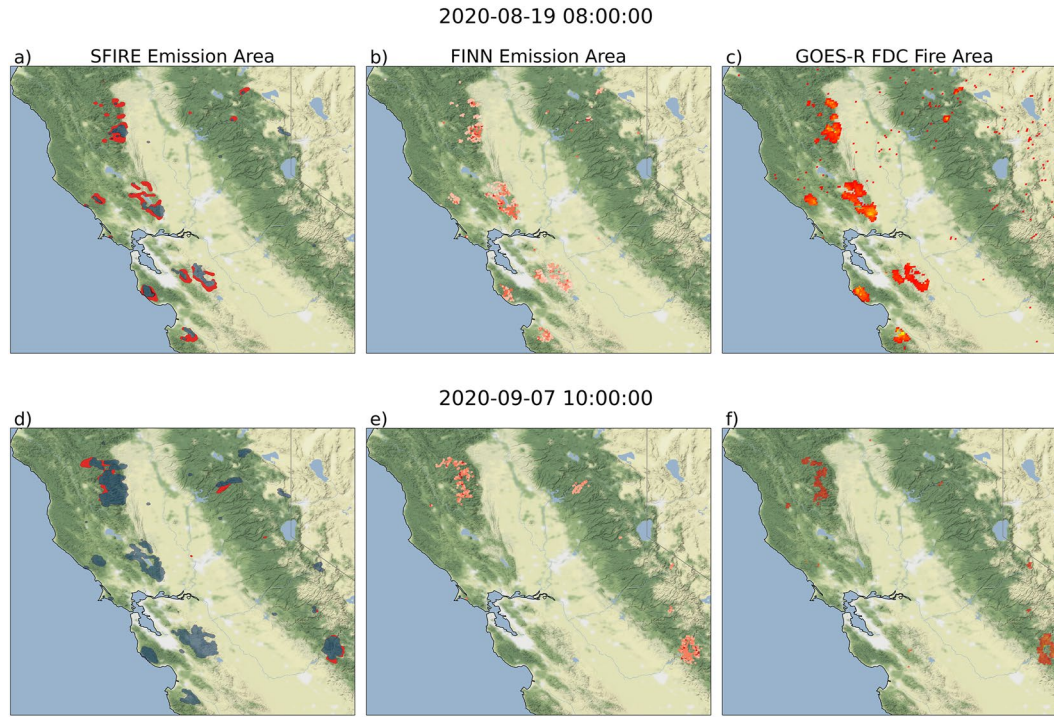


Figure 2. Snapshots of fire area from (a, d) SFIRE, (b, e) Fire Inventory from NCAR (FINN), and (c, f) GOES-17 fire detection products. The first row (a–c) shows fire area from 18 August at 0800UTC, the second row (d–f) from 7 September at 1000 UTC. The SFIRE panels (a, d) show the active fire area in red and the area with all fuel consumed in blue.

Burnup algorithm (Lutes, 2013; Reinhardt, 2003). The blue shaded regions in Figures 2a and 2d represent pixels where the fuel was fully consumed; these pixels were no longer capable of burning or producing smoke. In Figure 2d, the relatively large blue area indicates that these fires have burned over a large landscape and that the active fire area is comparatively small.

In contrast, the smoke simulations with FINN use a different set of simplifying assumptions. FINN fire locations are derived from MODIS fire detections. These fire detections are merged with MODIS landuse classification products to determine the type of fuel that is burning. From the MODIS landuse data product, each pixel is assigned a fractional coverage for each of 5 broad fuel classifications: boreal forest, tropical forest, temperate forest, woody savannah/shrubland, and savanna/grassland. For each FINN pixel with an active fire detection assigned to it, it is assumed that 100% of forest, 75% of grassland, and 0% of bare cover land classifications within that pixel are on fire. FINN does not account for previous fires leading to fuel consumption on a given pixel; as long as an active fire detection on a given pixel is present, then this propagates through FINN as an active fire, and the corresponding location in WRF-Chem can continue to emit smoke indefinitely. Practically, if the fire detection product is accurate, this can provide realistic inputs of smoke to the model at daily temporal resolution. However, given the uniform diurnal profile, the daily variability in emissions may not be accurately represented.

From Figure 2, a qualitative agreement is observed among the three different fire area estimates, with actively emitting fire pixels being grouped in similar parts of the map. In parts of the August Complex Fire, some of the pixels described as active fire locations according to FINN are colored blue in the respective SFIRE panel, indicating that these locations have exhausted their fuel supply. This difference can lead to an underestimation of emissions in SFIRE in the center of the fire. Because the purpose of this study is to compare out-of-the-box workflows for both the SFIRE and FINN approaches, we do not attempt to correct these issues here, but document them for future reference. We include the daily emissions locations with comparisons to GOES-17 fire detections for all days in our simulation period in Section S3.2 in Supporting Information S1.

To compare the fire area and associated emissions throughout the entire simulation, we plot the domain-integrated fire area and CO emissions fluxes in Figures 3a and 3b, respectively. For SFIRE simulations, area burn is computed by counting pixels where fuel is actively decreasing and multiplying this by the grid cell area. For

21698996, 2023, 6, Downloaded from https://agupubs.onlinelibrary.wiley.com/doi/10.1029/2022JD037062 by University Of California Irvine Science Library Serials, Wiley Online Library on [29/09/2026]. See the Terms and Conditions (https://onlinelibrary.wiley.com/terms-and-conditions) on Wiley Online Library for rules of use; OA articles are governed by the applicable Creative Commons License

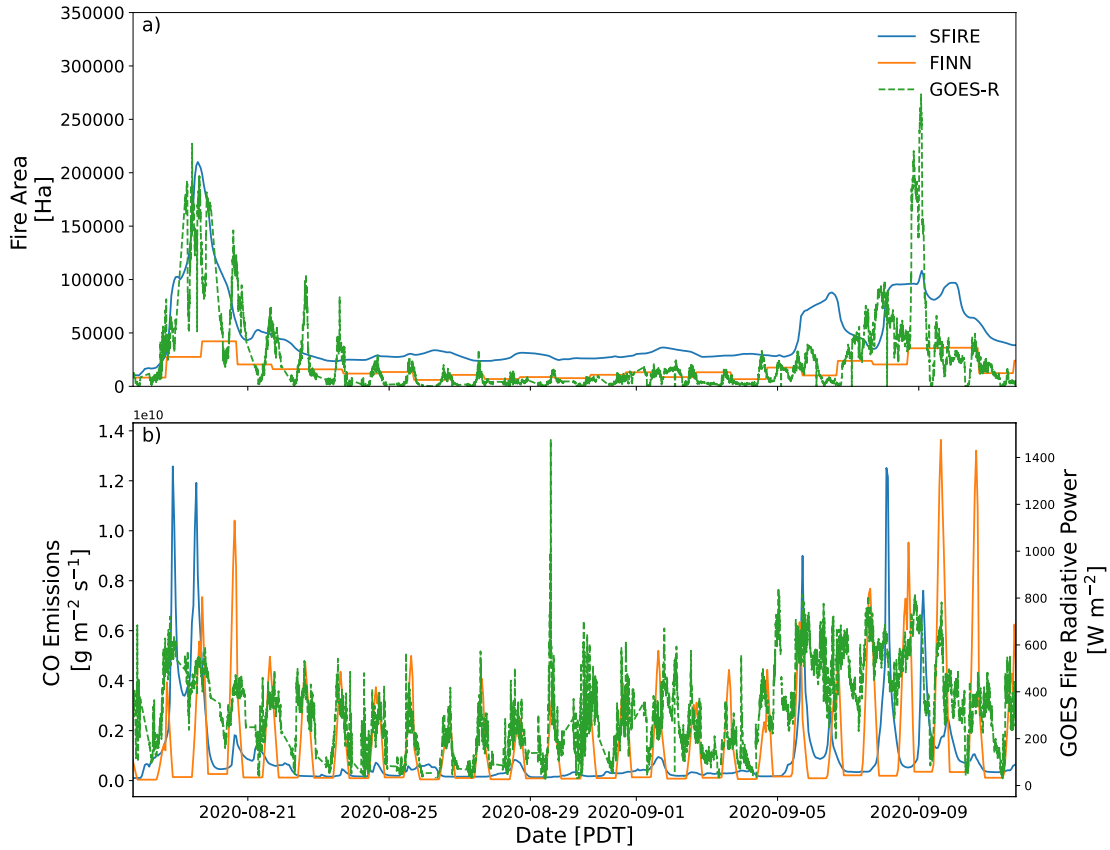


Figure 3. Comparison of SFIRE (blue), Fire Inventory from NCAR (FINN) (orange), and GOES-17 (green): (a) time history of domain-integrated fire area, and (b) CO emissions flux (from SFIRE and FINN, left *y*-axis_) and fire radiative power (from GOES-17, right *y*-axis).

FINN, the burn area is an input to WRF-Chem and can be read directly from the fire input files, and is computed based on the methodology outlined in Wiedinmyer et al. (2011). In Figure 3a, we overlay the GOES-17 FDC Fire Area. Because the GOES-17 FDC product does not include any information about emissions fluxes, we have instead overlaid the domain-integrated FRP in Figure 3b. The FRP is proportional to the emissions flux by the ratio of the heat of combustion to the chemical emissions factor; thus, whereas the units are different, we expect the FRP to be highly correlated with emissions fluxes (Schreier et al., 2014; Wiggins et al., 2020).

In Figure 3a, we observe that the fire area is correlated between FINN and SFIRE, but also that there are three key differences. First, SFIRE predicts an active fire area that is larger by a factor of approximately two than that predicted by FINN. This discrepancy is even larger around 20 and 21 August, when the wildfire complexes near SF were rapidly growing and merging. This result is not surprising because the SVM method, driven by relatively coarse satellite data, tends to overestimate the initial fire growth when the fire area is relatively small compared to the size of the satellite footprint (Farguell et al., 2021). Second, SFIRE allows for continuous changes in fire area to reflect the real-time fire spread, whereas FINN has a daily temporal resolution because it is derived from polar-orbiting remote sensing observations. The coarse temporal resolution results in very pronounced changes in the fire area at midnight as the next day's fire-detections are imposed. Finally, differences in timing of fire growth are observed during the Creek Fire period between 5 and 8 September: SFIRE shows rapid growth on 6 and 8 September, whereas FINN shows the increase occurring later.

The GOES-17 fire areas do not unambiguously show better agreement with either the FINN or SFIRE fire areas. Early in the time period, GOES-17 data agrees with the large increase in fire area that SFIRE predicts. During the middle of the period, GOES-17 data shows lower fire areas that more closely agree with FINN, although these data presents considerable diurnal variability in fire area and occasionally estimates larger burn areas than SFIRE. During the end of the period, the timing of the GOES-17 Creek Fire increase in burn area seems to better agree with FINN, and the area burned is roughly in between the two methods.

21698996, 2023, 6, Downloaded from https://agupubs.onlinelibrary.wiley.com/doi/10.1029/2022JD037062 by University Of California Irvine Science Library Serials, Wiley Online Library on [29/09/2026]. See the Terms and Conditions (https://onlinelibrary.wiley.com/terms-and-conditions) on Wiley Online Library for rules of use; OA articles are governed by the applicable Creative Commons License

21698996, 2023, 6, Downloaded from https://agupubs.onlinelibrary.wiley.com/doi/10.1029/2022JD037062 by University Of California Irvine Science Library Serials, Wiley Online Library on [29/09/2026]. See the Terms and Conditions (https://onlinelibrary.wiley.com/terms-and-conditions) on Wiley Online Library for rules of use; OA articles are governed by the applicable Creative Commons License

The GOES-17 fire area also includes a very large spike in fire area on September 9th which is not present in either of the two model runs. GOES-17 is a geostationary satellite, so it reports observations for changes in fire area during a given day, whereas FINN, from MODIS, has only a single fire area per day. However, GOES-17 is at a coarser spatial resolution than either FINN or SFIRE, which are at 1 km and 100 m respectively in this simulation. Furthermore, the extreme diurnal variability in GOES-17 fire areas may not be the result of actual physical variability; since GOES-17 uses near infrared (IR) wavelengths to detect fires, interference from solar radiation may lead to false positives that can artificially augment diurnal variations in fire activity (Hall et al., 2019). Additionally, dense smoke from the fires may have interfered with retrieved fire properties from both GOES and MODIS observations, though the impact may be different for each of the satellite products. Smoke interference in MODIS would propagate through to both FINN and the SVM-derived fire locations, though how this would impact these data fields is difficult to ascertain, and likely differs between fires. GOES-17 is still a relatively new satellite platform, and as its use becomes more widespread in the community, postprocessing routines which can account for these diurnal variations will become more mature. However, the large diurnal variability makes it difficult to conclude if FINN or SFIRE are in better agreement with GOES-17 in terms of total area burned.

The CO emissions fluxes plotted in Figure 3b show that the average emissions fluxes are greater for FINN than for SFIRE, despite SFIRE having a larger burn area. Both SFIRE and FINN emissions exhibit diurnal behavior. With FINN, the diurnal cycle is imposed on the fire activity by the WRF fire emis preprocessing routine; the hourly emissions flux is a rescaling of the total fire activity with close to zero emissions overnight, and a maximum emissions flux at 1 p.m. local time (Mu et al., 2011). This diurnal profile is the same each day, and is used to modulate the bulk emissions which are inferred from the MODIS fire detection and the underlying landuse classification. In contrast, SFIRE computes the emissions based on the advancing fire front, and the simplified Burnup algorithm for fuel consumption behind the fire front. The typical SFIRE diurnal cycle depends on model-calculated variables such as windspeed and relative humidity; therefore it varies from day-to-day depending on weather conditions. It is important to note that, in the SFIRE simulation analyzed here, the fire progression is constrained using the SVM-derived fire history, which impacts the temporal evolution of fire emissions.

Both SFIRE and FINN use the same set of emission factors, which relate the mass emissions of each smoke species (e.g., organic aerosol, NO_2, and CO) to the mass of fuel consumed. Therefore, the differences in SFIRE versus FINN emissions are a function of the differences in when and how much biomass undergoes combustion. During periods when SFIRE predicts rapid fire growth, emissions fluxes are considerably higher than FINN. However, during periods of little to no predicted fire growth, emissions are similarly zero. In this respect, SFIRE does not represent longer-term smoldering fire behavior. In contrast, FINN uses active fire detections to force fire emissions, and so emission are less correlated with rate of spread. The rate of biomass combustion is also correlated with the heat release and temperature of the fire, and therefore can be estimated from remotely sensed FRP. The overlaid GOES-17 FRP (Figure 3b, right *y*-axis) shows a pronounced diurnal cycle that more closely resembles the sharp FINN diurnal profile, especially in the middle of the time period. However, during periods of rapid growth, the GOES-17 FRP does not go to zero as the FINN emissions do. It is important to note that GOES-17 FRP, like fire area product, uses radiance in near IR wavelengths to distinguish fire pixels from surrounding vegetation, and may be subject to similar contamination by solar radiation as described above. The GOES-17 FPR daily maximum appears to be correlated with both FINN and SFIRE daily maximum emissions fluxes, although the FINN daily maximum diverges from the GOES-17 and SFIRE near the end of the simulated time period. As a result, it is difficult to conclude if the FINN or SFIRE emissions fluxes are more accurate.

In summary, the simulations using SFIRE to compute fire area generally predict larger burn areas when compared to FINN; however, due to differences in assumptions of fuel load and emissions, FINN simulations produce more emissions per area. The net effect of these differences is that SFIRE produces more emissions during time periods when fires grow rapidly, whereas FINN produces more emissions in the middle of the time period when fires are not undergoing rapid growth. Based on comparison to remote sensing data, it is difficult to conclude if the FINN or SFIRE representation of emissions fluxes more accurately reflect what occurred. However, it is useful to understand the differences of the model inputs, as this helps to explain differences in the simulation results.

4.2. Surface $PM_{2.5}$

In this section, we first analyze the surface smoke concentrations obtained from the different simulations. Following the standard practice in modeling studies of wildfire smoke, we use $PM_{2.5}$ at high atmospheric loadings as a

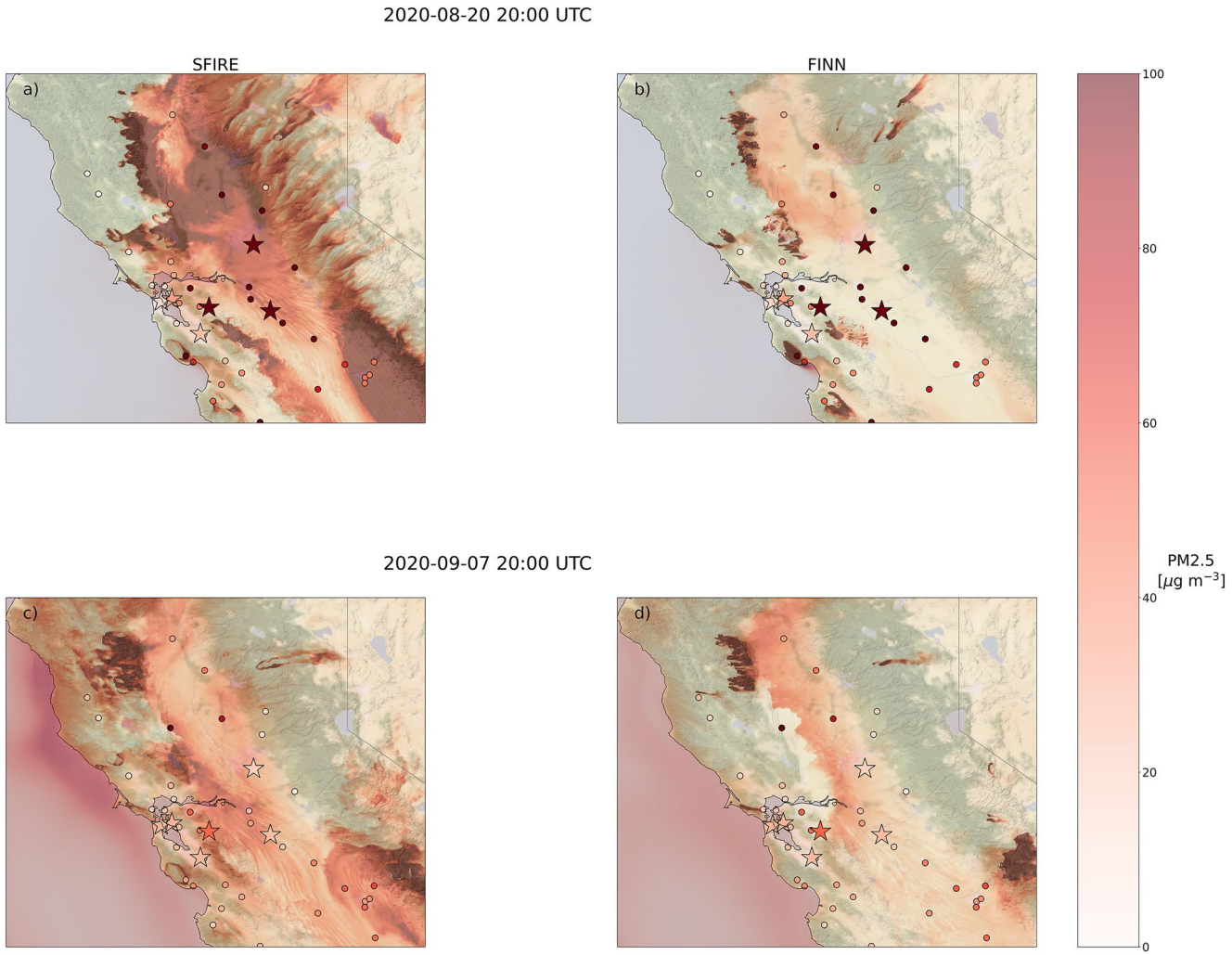


Figure 4. Plan view of surface $PM_{2.5}$ concentrations for SFIRE (a, c) and Fire Inventory from NCAR (FINN) (b, d) corresponding to two snapshots: 20 August at 2000 UTC (a, b) and 7 September at 1600 UTC (c, d). All panels have the corresponding EPA surface measurements overlaid as points with the same color scale. Black points are locations where the color map has fully saturated. Star shaped markers indicate the timeseries locations in Figure 5.

proxy for smoke. Furthermore, $PM_{2.5}$ is a National Ambient Air Quality Standard (NAAQS) criteria pollutant. California offers a comparatively dense network of surface monitors that allows effective validation of smoke simulations, while in general, the density of surface monitoring sites is insufficient for this application.

In Figure 4, we show surface $PM_{2.5}$ concentrations from SFIRE (Figures 4a and 4c) and FINN (Figures 4b and 4d) simulations at an early (20 August at 2000 UTC, Figures 4a and 4b) and late (7 September at 2000 UTC, Figures 4c and 4d) phase in the simulation periods, with the EPA AQS hourly surface measurements overlaid. It is observed that surface $PM_{2.5}$ concentrations are higher for the SFIRE simulation than for the FINN simulation at both times. During the first time period, surface monitor sites, especially in the central valley, indicate elevated smoke, suggesting that SFIRE is more accurate across the entire region at this time. However, SFIRE places the main central valley smoke plume east of the monitors that indicate elevated $PM_{2.5}$. This result may be due to small errors in model-simulated winds at the flame front, fire behavior and smoke emissions, plume rise, or other sources. With respect to the FINN simulation, the model appears to underpredict surface $PM_{2.5}$ concentrations at this time. Because this snapshot is from 2000 UTC (11 a.m. LDT), it represents an earlier time in the day than when most of the FINN emissions are specified to occur.

The second snapshot in Figures 4c and 4d shows that the SFIRE simulations predict more widespread $PM_{2.5}$ emissions across Northern California. However, the surface measurements at this time appear to be in better

21698996, 2023, 6, Downloaded from https://agupubs.onlinelibrary.wiley.com/doi/10.1029/2022JD037062 by University Of California Irvine Science Library Serials, Wiley Online Library on [29/09/2026]. See the Terms and Conditions (https://onlinelibrary.wiley.com/terms-and-conditions) on Wiley Online Library for rules of use; OA articles are governed by the applicable Creative Commons License

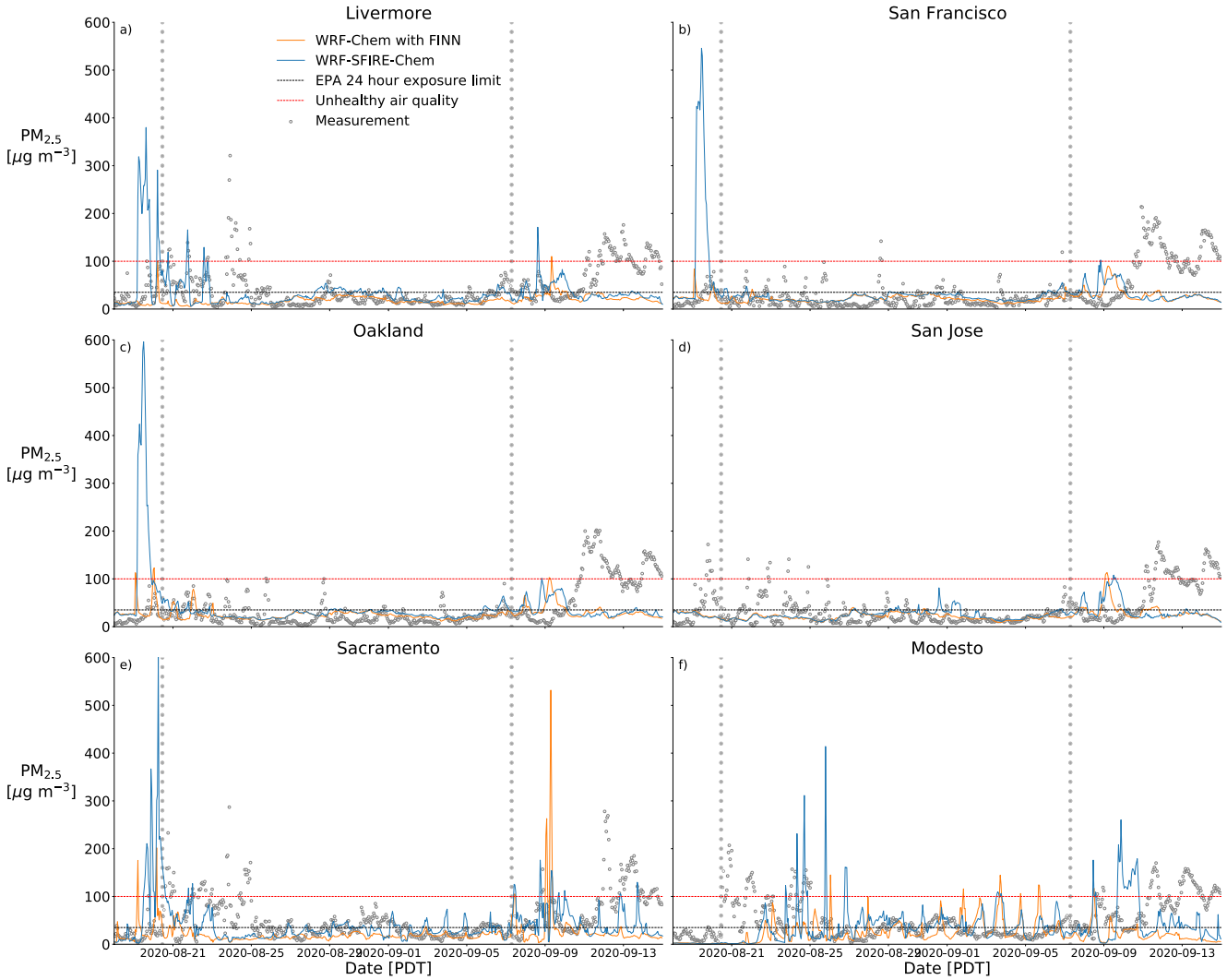


Figure 5. Timeseries plots of surface $PM_{2.5}$ from Weather Research and Forecasting model with Chemistry simulations with SFIRE (blue), and Fire Inventory from NCAR (FINN) (orange), alongside surface observations from EPA-AQS (points). Timeseries locations are (a) Livermore, (b) San Francisco, (c) Oakland, (d) San Jose, (e) Sacramento, and (f) Modesto. The times corresponding to the map plots in Figure 4 are indicated with vertical dashed lines.

agreement with the FINN surface $PM_{2.5}$ estimates, whereas SFIRE concentrations are significantly higher, especially in the SF Bay Area and central valley regions of the domain. Surface monitors close to the August Complex Fires in the northern part of the domain, and close to the Creek Fire in the southeastern part of the domain both indicate elevated $PM_{2.5}$, which agree better with SFIRE, or even exceed SFIRE predictions for these specific fires. Finally, in panel 4c, we observe some red outlines of the CZU and LNU fire perimeters directly south of the SF Bay area. These red outlines correspond to emissions from the fires' flaming fronts that continue to advance in SFIRE, which is an artifact of the SVM method used to constrain the fire progression. In these instances, the fires were known to be inactive, based on MODIS imagery or NIFC incident reprts. However, this version of the SVM method contains no mechanism to properly extinguish fires at the correct time, leading to these unrealistic ring structures of active fire around burn scars. Due to their size, these structures do not contribute a significant amount of $PM_{2.5}$ to the simulation domain. These fire perimeters are not present in the remote sensing data at this time, and therefore are not present in the FINN simulation, which agrees better with surface $PM_{2.5}$ concentrations.

In order to discuss the differences between these two simulations (SFIRE and FINN) during the entire simulated period, we overlay timeseries of surface $PM_{2.5}$ with measurements from a few key locations inside the simulation domain in Figure 5. Figures 5a–5d shows locations in the densely populated SF Bay Area and surrounding suburbs (i.e., Livermore, SF, Oakland, and San Jose); Figure 5e shows Sacramento, whereas Figure 5f shows

21698996, 2023, 6, Downloaded from https://agupubs.onlinelibrary.wiley.com/doi/10.1029/2022JD037062 by University Of California Irvine Science Library Serials, Wiley Online Library on [29/09/2026]. See the Terms and Conditions (https://onlinelibrary.wiley.com/terms-and-conditions) on Wiley Online Library for rules of use; OA articles are governed by the applicable Creative Commons License

21698996, 2023, 6, Downloaded from https://agupubs.onlinelibrary.wiley.com/doi/10.1029/2022JD037062 by University Of California Irvine Science Library Serials, Wiley Online Library on [29/09/2026]. See the Terms and Conditions (https://onlinelibrary.wiley.com/terms-and-conditions) on Wiley Online Library for rules of use; OA articles are governed by the applicable Creative Commons License

Modesto, a medium-size city in the central valley. Figure 5 also reports the EPA 24-hr $PM_{2.5}$ exposure limit of 35 μg m^{-3} as a black dashed line, and the EPA AirNow "hazardous air quality" limit of 100 μg m^{-3}. It is important to note that EPA limits only apply to anthropogenic contributions to criteria pollutant concentrations, and the 35 μg m^{-3} limit is for 24-hr average concentrations and we have plotted hourly concentrations. Nevertheless, we find this helpful for providing context for the simulated and observed $PM_{2.5}$ concentrations. These sites are selected to give a range of examples of the types of communities that were impacted by smoke; however, similar figures for all of the available measurement sites inside our simulation domain are provided in Section S2.2 in Supporting Information S1.

In Figures 5a–5c, and 5e, the SFIRE simulation suggests a very significant increase in surface $PM_{2.5}$ concentrations, with values as high as 600 μg m^{-3} at the beginning of the time period. Both FINN and the surface observations show increases in concentrations at this same time; however, these increases are much smaller in magnitude. This spike in surface $PM_{2.5}$ is temporally linked with the large increase in fire area, shown in Figure 2a. The fires during this period were dominated by wildfire complexes that grew and merged together. These conditions are difficult to reproduce with the SVM algorithm used in the SFIRE simulation, because this algorithm is based on relatively coarse satellite data. It is possible that the fire arrival times derived from the SVM algorithm prescribed initial growth that was more rapid than what was observed. Additionally, it is likely that the Burnup algorithm produced artificially fast rates of fuel consumption. The combination of these two factors most likely produced the observed large spike in $PM_{2.5}$ emissions.

Based on the provided timeseries plots, it is noteworthy that neither simulation captures the observed elevated $PM_{2.5}$ that occurred during the final few days of the simulation. The smoke during this period was transported from fires that occurred near Portland, OR, which was outside of our innermost WRF domain (D03), but included in the next coarsest domain (D02). It should be noted that there is no difference in the representation of these remote fires in the FINN and SFIRE simulations, as both simulations use the FINN fire and emissions treatment outside of D03. Thus, whereas the Portland fires are simulated with FINN on D02 at 3 km resolution, the model fails to represent the long-range transport of smoke from Oregon to our area of study, as further discussed in Section S2.2 in Supporting Information S1.

In order to quantify the relative model skill for SFIRE and FINN simulations, Figure 6 contains 1:1 plots comparing the simulated daily mean $PM_{2.5}$ for SFIRE and FINN (Figures 6a and 6c) as well as the daily maximum $PM_{2.5}$ concentrations (Figures 6b and 6d) from all measurement sites. Overlaid on top of the data is a $y = x$ line, corresponding to perfect agreement between the simulated and observed values of $PM_{2.5}$ concentrations. Two cutoff criteria are selected as a basis for binary classifier analysis: 35 μg m^{-3} for daily average (based on the EPA NAAQS 24-hr limit for $PM_{2.5}$), and 100 μg m^{-3} (corresponding to an Air Quality Index of "unhealthy") for daily maximum. In Figure 6, blue denotes True Positive results, orange denotes False Positive results, purple denotes True Negative results, and red denotes False Negative results. Table 1 contains a summary of the associated binary classification metrics.

The high $PM_{2.5}$ bias in the SFIRE simulations results in a greater probability of $PM_{2.5}$ concentrations exceeding the daily average and daily maximum thresholds. Consequently, the SFIRE simulation has a higher True Positive Rate (TPR) and False Positive Rate (FPR), but lower True Negative Rate (TNR) and False Negative Rate (FNR) as compared to the FINN simulation. However, when aggregated, these differences cancel each other out. In fact, both simulations have nearly identical Positive Predictive Value (PPV, defined as the number of true positives divided by the number of total total positives) and Negative Predictive Value (NPV, defined as the number of true negatives divided by the number of total negative results), with the only exception being PPV for daily maximum $PM_{2.5}$, for which the SFIRE simulation presents slightly higher values. Both simulations have a stronger NPV than PPV, with this discrepancy being more pronounced for predicting hazardous daily maximum $PM_{2.5}$ concentrations. Essentially, both of these modeling tools currently are more accurate in predicting no-smoke conditions than high-smoke conditions. The F1 scores, defined as $\mathbf{2 \cdot PPV \cdot NPV/(PPV + NPV)}$, are identical for the binary classification analysis for daily average $PM_{2.5}$. However, for the daily maximum binary classification analysis, the SFIRE simulation slightly outperforms the FINN simulation. In all cases, the F1 scores are relatively low. Binary Classification analysis is widely used approach for incorporating wildfire smoke estimates from chemical transport models into response (Ainslie et al., 2022), which is why we used it here. Furthermore,

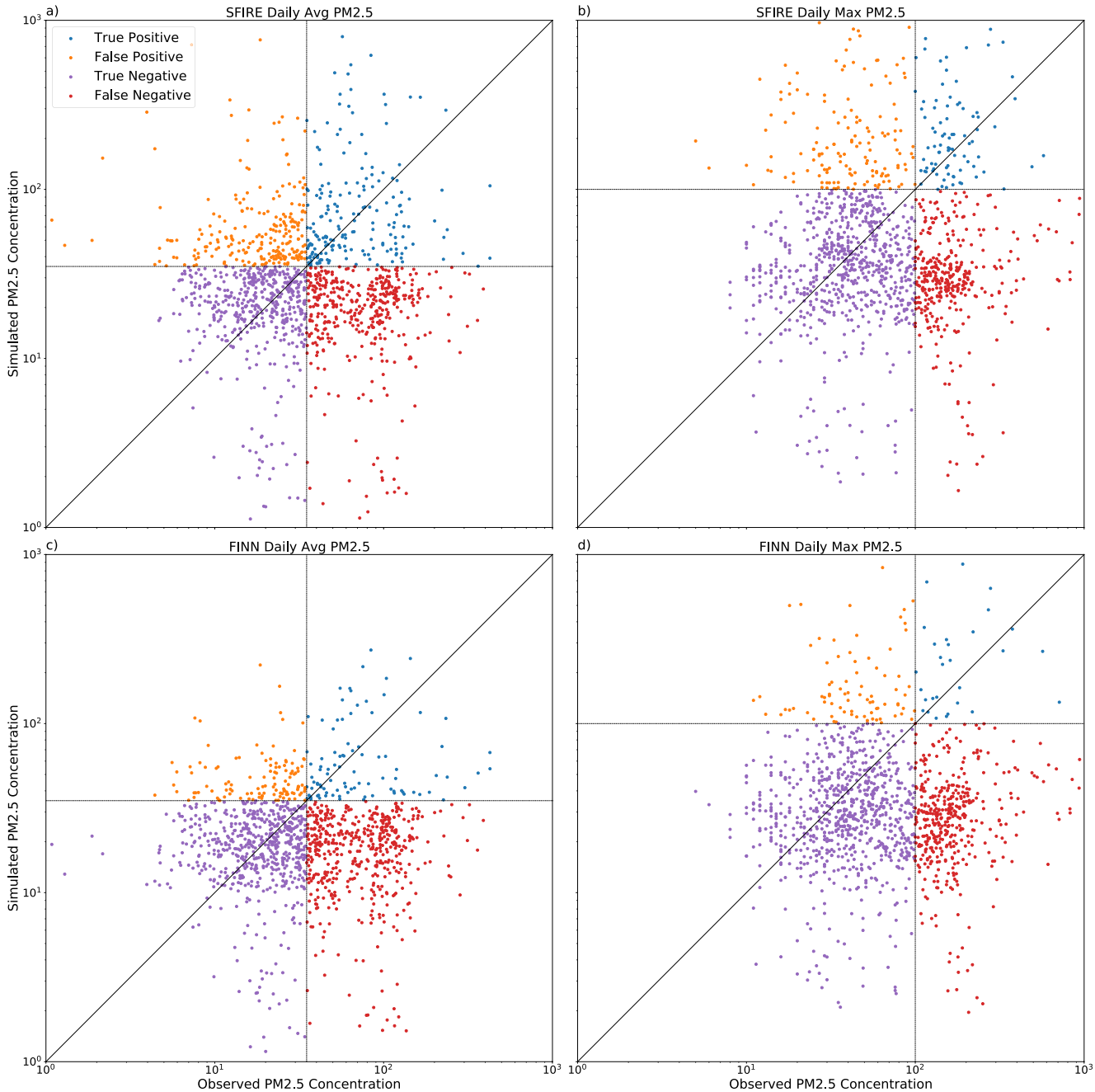


Figure 6. Comparison of simulated (*y*-axis) and observed (*x*-axis) $PM_{2.5}$ concentrations: (a) SFIRE daily averages, (b) SFIRE daily maxima, (c) Fire Inventory from NCAR (FINN) daily averages, and (d) FINN daily maxima. Either daily National Ambient Air Quality Standard exceedance (a, c) or concentrations equivalent to an hazardous air quality index (b, d) are overlaid as gray lines. All panels include the $y = x$ line corresponding to perfect agreement between simulation and field observations. Points are colored according to True Positive = blue (i.e., model correctly predicts high $PM_{2.5}$ concentration), False Positive = orange (i.e., model incorrectly predicts high $PM_{2.5}$ concentration), True Negative = purple (i.e., model correctly predicts low $PM_{2.5}$ concentration), or False Negative = red (i.e., model incorrectly predicts low $PM_{2.5}$ concentration), according to the binary classification criteria for average and maximum concentrations.

due to the sharp gradients present in wildfire smoke simulations, more traditional analysis of correlation, mean bias, and root mean square error typically produce poor results (Lassman et al., 2017). This can increasingly penalize models at higher resolution even if the simulated plume is more realistic, as coarse resolution artificially smooths steep concentration gradients (Lassman, 2015).

21698996, 2023, 6, Downloaded from https://agupubs.onlinelibrary.wiley.com/doi/10.1029/2022JD037062 by University Of California Irvine Science Library Serials, Wiley Online Library on [29/09/2026]. See the Terms and Conditions (https://onlinelibrary.wiley.com/terms-and-conditions) on Wiley Online Library for rules of use; OA articles are governed by the applicable Creative Commons License

21698996, 2023, 6, Downloaded from https://agupubs.onlinelibrary.wiley.com/doi/10.1029/2022JD037062 by University Of California Irvine Science Library Serials, Wiley Online Library on [29/09/2026]. See the Terms and Conditions (https://onlinelibrary.wiley.com/terms-and-conditions) on Wiley Online Library for rules of use; OA articles are governed by the applicable Creative Commons License

Table 1
Binary Classification Statistics for SFIRE and Fire Inventory From NCAR Simulations Containing True Positive Rate (TPR), False Positive Rate (FPR), True Negative Rate (TNR), False Negative Rate (FNR), Positive Predictive Value (PPV), Negative Predictive Value (NPV), and F1 Score for Daily Mean and Daily Maximum $PM_{2.5}$ Concentrations

	Simulation	TPR	FPR	TNR	FNR	PPV	NPV	F1 score
Daily mean	SFIRE	0.32	0.34	0.66	0.68	0.43	0.55	0.24
	FINN	0.15	0.17	0.83	0.84	0.43	0.55	0.24
Daily max	SFIRE	0.21	0.19	0.81	0.79	0.36	0.67	0.23
	FINN	0.07	0.09	0.91	0.92	0.27	0.66	0.20

4.3. Satellite-Derived AOD

To assess the accuracy of the smoke simulations, we compare the simulation results to satellite observations of smoke plumes. In Figure 7, we plot the SFIRE AOD (left column), the FINN AOD (center column), and the MODIS AOD (right column). We show snapshots corresponding to the Terra satellite overpass (approximately 11 a.m. LST) on four different days: 21, 31 August and 5, 9 September 2020.

Throughout the simulated period, the MODIS AOD retrieval on any given day has many pixels with missing data. AOD retrievals are calibrated for typical ambient aerosol concentrations, whereas smoke is often an extreme event; in this context, bright smoke is often mistaken for clouds and erroneously flagged by the retrieval. This issue is further complicated on the west coast of the US, which often has dense stratus clouds and onshore fog,

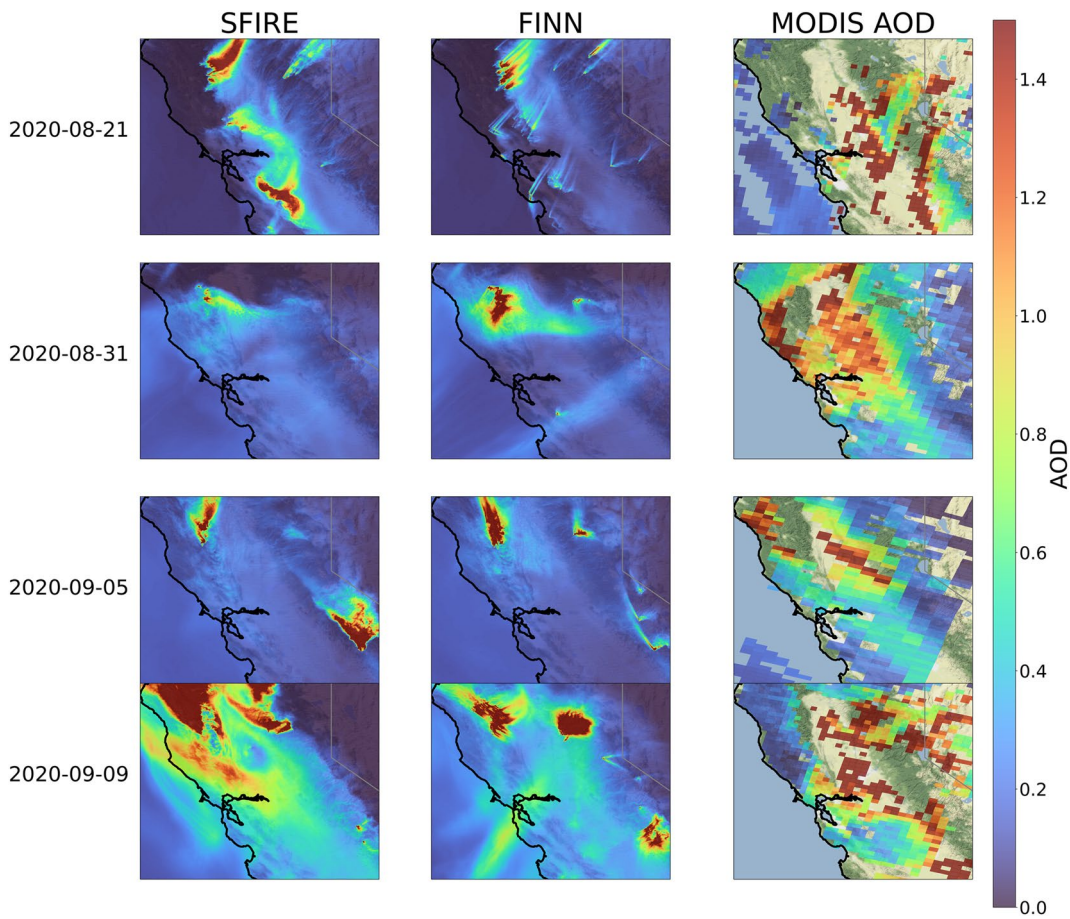


Figure 7. Aerosol Optical Depth (AOD) from SFIRE simulations (left column), Fire Inventory from NCAR (FINN) simulations (center column), and Moderate Resolution Imaging Spectroradiometer observations (right column) taken from 21 August (first row), 31 August (second row), 5 September (third row), and 9 September (fourth row).

21698996, 2023, 6, Downloaded from https://agupubs.onlinelibrary.wiley.com/doi/10.1029/2022JD037062 by University Of California Irvine Science Library Serials, Wiley Online Library on [29/09/2026]. See the Terms and Conditions (https://onlinelibrary.wiley.com/terms-and-conditions) on Wiley Online Library for rules of use; OA articles are governed by the applicable Creative Commons License

or exposed ocean, all of which can be problematic for AOD retrievals. The dates shown in Figure 7 are chosen to provide a sufficient coverage to visibly identify thick smoke plumes. Gaps in the center of smoke plumes can reasonably be assumed to contain additional smoke.

In general, it is difficult for WRF-Chem simulations to reproduce MODIS AOD. Balzarini et al. (2015) found that WRF-Chem/MODIS AOD relationships can be a strong function of the chemical mechanism for both gas and aerosol phases, and Karumuri et al. (2022) found that the relative bias between WRF-Chem and MODIS AOD can vary regionally within the simulation domain. However, some studies have had success reproducing MODIS AOD with WRF-Chem simulations (e.g., Chen et al., 2014; Siméon et al., 2021). Both of these studies used MOZCART gas and aerosol phase mechanisms in WRF-Chem to simulate wildfire smoke and showed good agreement with remotely sensed AOD. However, Siméon et al. (2021) used multiple simulations to refine the speciation of aerosol emissions and organic carbon/black carbon ratios, as well as aerosol optical properties, while Chen et al. (2014) used an AOD data assimilation process to constrain their simulations. Furthermore, both of these studies were conducted at coarse spatial resolution (20×20 and 30×30 km^2, respectively). Lassman (2015) found that using MODIS to evaluate high-resolution simulations leads to large errors, with model simulations typically biased high; however, for high resolution, the agreement becomes more binary and qualitative. Due to the challenges associated with these kinds of model-measurement comparisons, we interpret MODIS AOD as an additional qualitative indicator of the spatial extent of the smoke plume, rather than a the basis for a quantitative assessment of simulation accuracy. In our simulations, we find that MODIS AOD is elevated over a larger area than both simulations suggest. Both WRF-Chem simulations show larger AOD values near fires, with smaller impacts on AOD regionally. From the data presented in Figure 7, it is difficult to determine if this is due to a systematic bias in WRF-derived AOD relative to MODIS AOD, or if this is a difference in the smoke dispersion. The spatial resolution of the MODIS AOD retrieval product is 10 km, which is much coarser than either model simulation, and thus unable to represent some of the sharper gradients that are present in the simulated quantities. It is possible that WRF-Chem is simply biased low relative to MODIS in computing the extinction coefficients and subsequent AOD calculation. One useful insight from the MODIS retrievals is that SFIRE seems to predict the smoke from the Creek Fire too early. AOD values are elevated in SFIRE on September 5th in the southeastern corner of the domain where the Creek Fire occurred. This observation is not reflected in the FINN simulation or in the MODIS AOD data. However, the FINN simulation also seems to show more Creek Fire activity on 9 September than on 5 September, which is in better agreement with the MODIS retrieval.

4.4. Fire-Weather Interactions

Dense smoke has been shown to impact surface temperatures by attenuating solar radiation and decreasing surface insolation (Robock, 1991; Stone et al., 2011). Additionally, smoke can impact cloud microphysics by changing the number of available cloud condensation nuclei (Kaufman & Nakajima, 1993). These processes are well-understood at global climate scales, known as the aerosol indirect effect and the aerosol semi-direct effect, impacting cloud brightness and cloud lifetime, respectively. Changes to the aerosol load can also have large impacts on convection (Heikenfeld et al., 2019). During normal ambient aerosol conditions, these effects are minimal; however, during intense smoke events, they can become large. For example, during the event considered in this study, dense smoke from fires obscured the sun, lowering surface air temperatures considerably. Because smoke-radiation and smoke-cloud effects are computationally expensive to simulate, these processes are not included in operational forecasting models. Consequently, although the effect was well documented in forecast discussions (Herzmann, 2020), NWS Forecasts routinely overpredicted surface temperatures by as much as 8°C.

The WRF-Chem smoke simulations presented in this work attempt to capture the complex effects of dense smoke on surface temperature by leveraging the unique capabilities of WRF-Chem to simulate the interactions between smoke aerosols and meteorology. Figures 8a and 8b show the temperature estimate bias for the SFIRE simulation at all available measurement sites for the early period (16–25 August 2020) and late period (5–12 September 2020) of the simulation. Over both time periods, the simulation significantly overestimated the surface temperature in the Central Valley. This is similar location to where the model failed to correctly predict the elevated AOD, suggesting that the simulations did not correctly place the smoke in the domain to achieve the correct magnitude of cooling. We also show the timeseries of observed temperatures from Oakland early in the time period (Figure 8c), and from Reno late in the time period (Figure 8d), compared with the simulated temperature obtained using the SFIRE, FINN, and NoFire simulations, with the last one representing the weather in the absence of

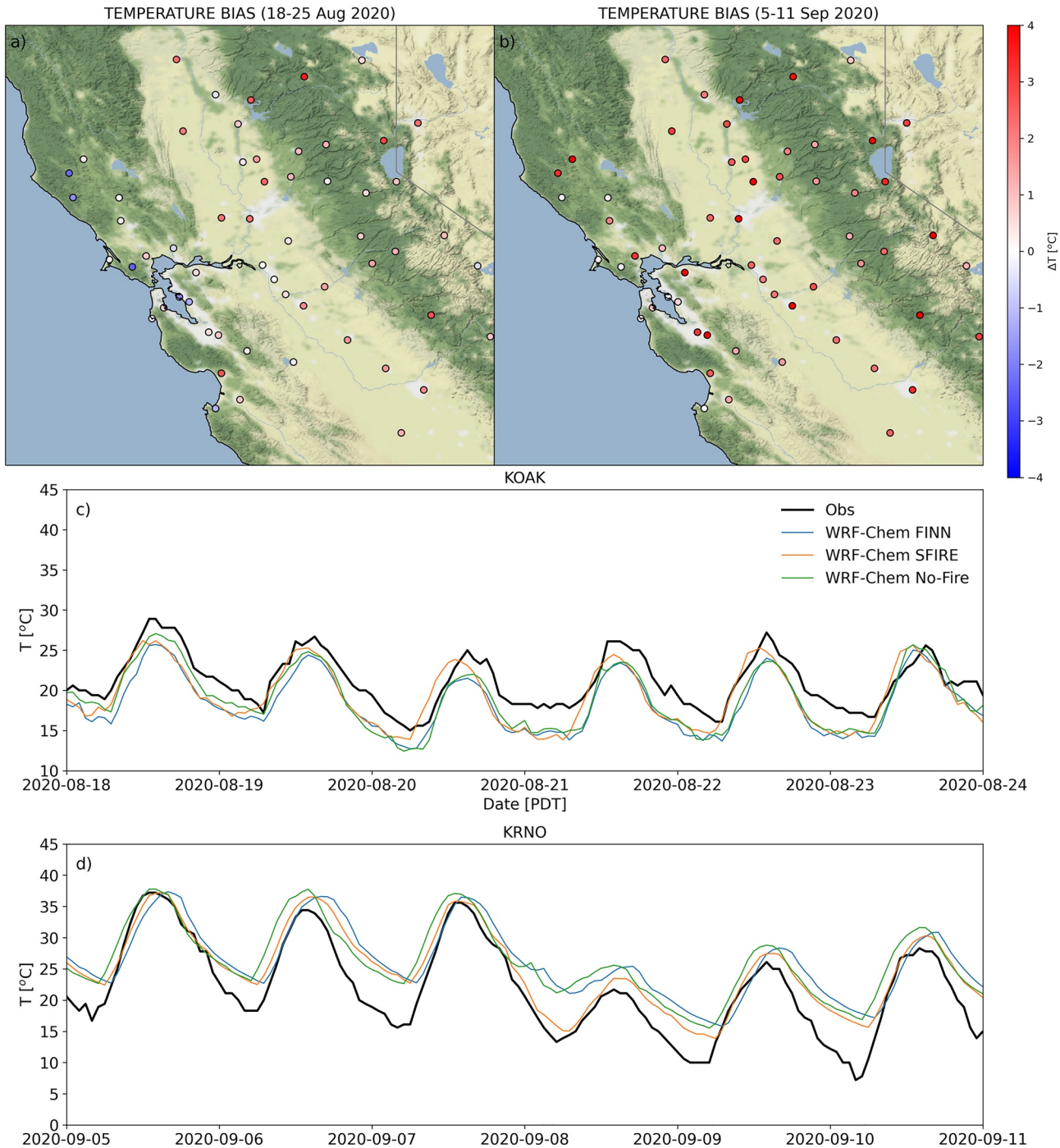


Figure 8. Temperature measurements and simulation estimates. (a and b) show the surface temperature bias for the SFIRE simulation from the beginning of the time period (16–25 August) and the end of the time period (5–12 September) respectively. (c and d) show the timeseries of surface temperatures measurements compared to the estimates obtained using the different model simulations. In particular, (c) shows the temperature data from Oakland, CA, during the beginning of the time period, and (d) shows the temperature data from Reno, NV, during the second half of the time period.

smoke effects. It is observed that including smoke improves the temperature estimates only when the smoke is in the correct part of the domain. In Reno, the SFIRE simulation improves the temperature performance from 7 to 9 September, but otherwise the models all return the same high-bias solution. During the beginning of the time period, the models have a low bias near the ocean, which is surprising given that the expected result is an overprediction of surface temperature due to failure to account for smoke shading of incoming sunlight. In the

21698996, 2023, 6, Downloaded from https://agupubs.onlinelibrary.wiley.com/doi/10.1029/2022JD037062 by University Of California Irvine Science Library Serials, Wiley Online Library on [29/09/2026]. See the Terms and Conditions (https://onlinelibrary.wiley.com/terms-and-conditions) on Wiley Online Library for rules of use; OA articles are governed by the applicable Creative Commons License

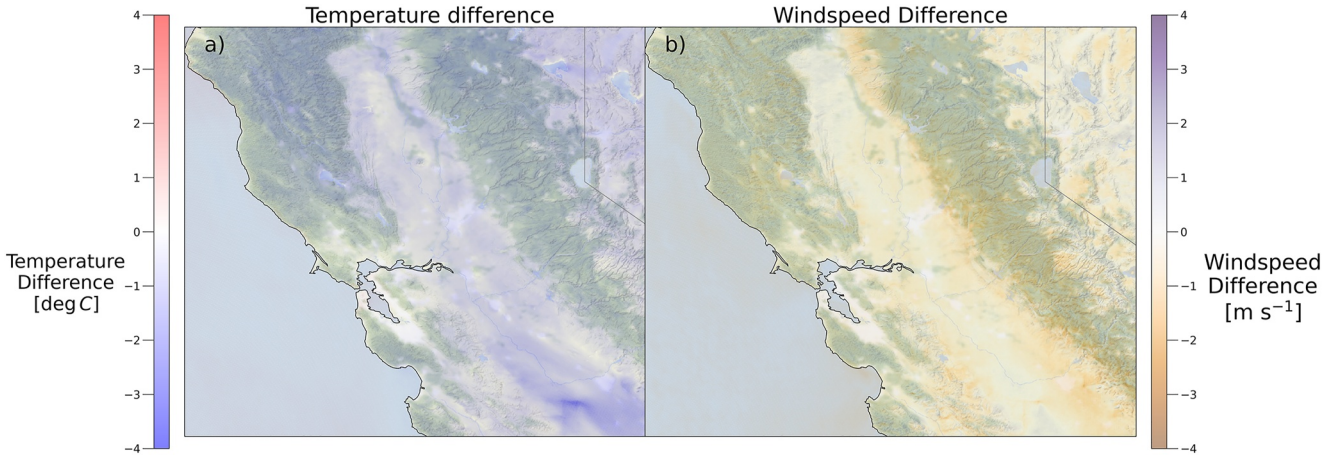


Figure 9. Comparison of SFIRE and NoFire simulations: (a) surface temperature difference, and (b) surface wind speed difference. Values are averaged over the entire simulation period.

temperature timeseries from Oakland, the primary model error is a nighttime underprediction, rather than the expected overprediction seen during the day. While it is well-known that smoke shading can lead to daytime overprediction of temperatures, it is less common for simulations to underpredict surface temperature as a result of smoke being present in the domain, implying that these interactions may be more complex. We speculate that this may in fact be due to smoke impacting the typical meteorological circulations in this region that are driven by orographic and marine circulations. To investigate this further, we compare the WRF-SFIRE-Chem simulation to the No-Fire simulation.

In Figure 9, we show the difference in temperature (Figure 9a) and windspeed (Figure 9b) between the SFIRE and NoFire simulations, averaged throughout the entire time period of the simulation. During the month-long simulation, the onshore temperatures are generally lower in the SFIRE simulation, with larger decreases occurring in the Central Valley, specifically in the southern section of the domain. Over the Sierra Nevada mountains to the east of the Central Valley, as well as along the coast, temperature effects from smoke appear to be weaker. Because the sea surface temperature is prescribed in these simulations, little change to the surface temperature is observed over the ocean. It is important to note that the ocean heat capacity is much larger than that of the land surface; thus, sea surface temperatures are expected to respond slowly to changes in solar flux due to smoke shading. Furthermore, the ocean in this region is typically covered in thick stratus clouds during this time of year, so any changes to sea-surface temperature due to attenuation of solar radiation would be minimal.

Concurrent with the average temperature decrease in the SFIRE simulations, a reduction in the average windspeed is also observed, especially in the Sierra Nevada mountains and between the Central Valley and the coast. In this region, high summer temperatures in the Central Valley during summer typically produce unstable air, producing convection and convergence. This phenomenon leads to a regional scale sea-breeze circulation whereby cold moist air from the Pacific Ocean advects onshore. Due to the presence of smoke in the valley, this circulation is weakened, reducing the magnitude of the onshore flow, leading to a decrease in windspeed. The windspeed decrease shown above is primarily due to changes in the zonal wind (i.e., the U component of the winds). These dynamics may help to explain the lack of temperature difference near the coast for the SFIRE simulation. In typical conditions, the presence of foggy air along the coast keeps surface temperatures cool. However, the presence of smoke also obscures the sun along the coast, resulting in a small temperature difference between the SFIRE and NoFire simulations. While these results lend some support to our hypothesis that the presence of smoke in the simulation interfered with the marine-driven circulations, more evidence, and a more targeted study, possibly with a coupled sea surface temperature model, are required to fully understand the mechanisms that may be at play and their implications.

4.5. Synthesis, Limitations, and Recommendations for Future Studies

In this study, we compare WRF-Chem simulations that use SFIRE and FINN to describe biomass burning emissions (SFIRE and FINN simulations, respectively) with each other, and with available observations. As expected,

21698996, 2023, 6, Downloaded from https://agupubs.onlinelibrary.wiley.com/doi/10.1029/2022JD037062 by University Of California Irvine Science Library Serials, Wiley Online Library on [29/09/2026]. See the Terms and Conditions (https://onlinelibrary.wiley.com/terms-and-conditions) on Wiley Online Library for rules of use; OA articles are governed by the applicable Creative Commons License

21698996, 2023, 6, Downloaded from https://agupubs.onlinelibrary.wiley.com/doi/10.1029/2022JD037062 by University Of California Irvine Science Library Serials, Wiley Online Library on [29/09/2026]. See the Terms and Conditions (https://onlinelibrary.wiley.com/terms-and-conditions) on Wiley Online Library for rules of use; OA articles are governed by the applicable Creative Commons License

the FINN and SFIRE simulations produce different results; however, it is not clear if one simulation outperforms the other. WRF-SFIRE with the SVM leveraging MODIS fire detections offers a new pathway for deriving highly accurate fire locations and timing. However, because WRF-SFIRE was developed originally as a fire spread model, it uses a comparatively simple fire emissions representation that relies on generic input data and parameters. Despite this, it is noteworthy that the SFIRE model provides results that are comparable to the more-established FINN emission inventory. By improving the representation of chemical and heat fluxes in SFIRE, especially behind the advancing flaming front, we may be able to develop a more-accurate strategy for simulating smoke from wildfires. We also investigate the effect of smoke on surface temperature and windspeed by comparing the SFIRE and FINN simulations to a WRF-Chem simulation with no smoke (i.e., NoFire simulation). These results are used to better understand the context behind the SFIRE and FINN simulation results, what these tools are designed to do, and what can be done to improve future coupled wildfire-air quality simulations.

FINN is a global emissions inventory. It uses real-time MODIS fire detections and pre-existing MODIS land-cover classification data to estimate fire location, area, and fuel type. FINN is used with a climatological diurnal profile for emissions because it is meant to provide information for a large number of fires. The workflow for a WRF-Chem simulation using FINN is identical independent of the size of the domain or the number of simulated fires. However, any individual fire event may not conform to these climatological assumptions; thus FINN can produce inaccurate estimates of emissions location, timing, and/or intensity. Previous studies (Lassman, 2015; Lassman et al., 2017) found that running WRF-Chem for a smaller number of wildfires in Colorado, or a larger number of fires in Washington state (2015 and 2017 respectively) did not produce smoke estimates with a high degree of skill. However, other studies have used FINN to achieve higher degrees of accuracy, and FINN itself has been updated since these simulations were performed. Given the nature of the FINN model inputs and workflow, there is little opportunity for parameter tuning or other adjustments that could easily lead to improved predictions for a given wildfire.

In contrast, SFIRE is designed for modeling the progression of a fire with time. Because it does not rely on assumed diurnal behavior, this method has the potential to be more accurate; however, this model is characterized by errors inherent to the fire progression model and the simplified Burnup model, as well as uncertainty in many of the model inputs. SFIRE also resolves plume rise instead of using an external parameterization, adding another degree of freedom linked to the fire behavior. Consequently, SFIRE can require more hands-on optimization or constraining of fire progression in order to produce an accurate prediction. Results from earlier simulations of multiple 2015 California fires (Kochanski et al., 2019), as well as a later study leveraging WRF-SFIRE to provide emissions and smoke plume parameters to the CMAQ model (Kochanski et al., 2021), reported good agreement between the simulated and observed plume top heights. It is possible that the explicit representation of plume dynamics in SFIRE may compensate for the limitations of the simple emission model, leading to results that are comparable to those obtained using FINN emissions.

Work by Farguell et al. (2021) represents a major breakthrough with the ability to perform simulations with fire progression simulations constrained using satellite observations. By using the SVM model to interpolate remotely sensed fire detections and derive fire arrival times, the simulated SFIRE fire progression is forced toward a solution that is consistent with the observed fire behavior. Furthermore, this workflow allows objective optimization of the simulation, assuring that the fire progression driving fire emissions is realistically represented. The SVM model has some limitations; for example, the initial fire area may be overestimated, especially when the fires are relatively small or have complex shapes that are difficult to map using relatively coarse satellite detections. However, such errors could be reduced as the approach is improved. In this study, the SVM algorithm ingested only polar-orbiting satellite-based fire detections, which are available at daily temporal resolution. However, in future studies, satellite products available at higher temporal frequency, such as FDC products from GOES-17, could be extremely useful for enhancing this strategy. Furthermore, GOES-18 may offer some enhanced capabilities that may be more useful for generating high-time-frequency insights about fire behavior.

Another important difference between SFIRE and FINN is the treatment of biomass consumption. FINN uses a top-down approach in which biomass conservation is ignored; in fact, the rate of emissions is directly correlated with the assumed diurnal profile, and is only a function of the MODIS landcover classification. In principle, if a real wildfire fully depletes the combustible fuel on a MODIS pixel, then no subsequent fire detections are possible on this grid cell, and the grid cell is completely "burnt up." This negates the need to track fuel consumption with time, which is a challenging quantity to remotely sense. Additionally, FINN is able to represent a grid cell

21698996, 2023, 6, Downloaded from https://agupubs.onlinelibrary.wiley.com/doi/10.1029/2022JD037062 by University Of California Irvine Science Library Serials, Wiley Online Library on [29/09/2026]. See the Terms and Conditions (https://onlinelibrary.wiley.com/terms-and-conditions) on Wiley Online Library for rules of use; OA articles are governed by the applicable Creative Commons License

that smolders for long periods of time; however, due to the assumed emissions profile, FINN almost always leads to an overprediction of emissions in this situation.

In SFIRE, each grid cell has a preexisting biomass as a function of fuel type. Pre-fire fuel load is an uncertain value, and having accurate and up-to-date estimates is often impossible for significant fires. This mass is a generic assumed value that is identical for all fuels of the same fuel type, and is thus lacking in precision, and could be a source of error and bias in the estimates of smoke emissions. Furthermore, the mass consumption is calculated according to the simplified Burnup algorithm (Lutes, 2013). The rate of spread computations are mostly controlled by fine fuels, and WRF-SFIRE is designed to estimate fire propagation. However, the smoke emissions are typically dominated by the slower combustion of coarse fuels, woody debris, and duff. The model resolves flaming emissions, but neglects residual smoke production after the fire front passage. Consequently, SFIRE emissions behind the advancing fire front may be underestimated, because the model does not represent slower fuel consumption in smoldering conditions. This limitation leads to an underprediction of total emissions for longer-living fire events, and to unrealistic ring-shaped emission with no smoke production coming from inside the fire perimeters.

Because the current SFIRE approach uses relatively generic data, it presents an opportunity to improve the fidelity with which SFIRE can compute smoke emissions. By using more precise inputs in terms of fuel load in various fuel layers and post-fire fuel mass to determine mass consumption, the mass of total emissions could be better constrained. Alternatively, by relating integrated FRP from a given fire, one could constrain mass consumption, which also could be used to constrain emissions. Likewise, FRP could also be used to inform the rate of mass consumption, which could be used to improve on the assumed exponential decay of fuel mass that is imposed by the Burnup algorithm. Alternatively, by using more detailed biomass combustion kinetics, a more detailed parameterization for fuel consumption could be derived, although this last approach would require a significant scientific effort.

5. Conclusions

The California 2020 wildfire season is the worst fire season on record, with over 1.5 million hectares of land consumed by fires. During this season, a record number of structures were threatened by fire, and a large percentage of the population, in California and downwind, were exposed to smoke. To study these effects, we conducted WRF-Chem simulations over a region that included most of Northern and Central California for a 1-month period during the 2020 California wildfire season. These simulations included chemical inputs from wildfires, anthropogenic and biogenic sources, with initial and boundary conditions from a global CTM. We compared model results obtained by combining WRF-Chem with a biomass burning emissions inventory (FINN) and with a coupled fire spread model (SFIRE).

FINN is an emissions inventory designed for investigating global wildfires on larger timescales, whereas SFIRE is a fire spread model designed for analyzing individual fires. These two approaches use different frameworks for determining fire location and fire activity, as well as for computing mass consumption rate of fuel; however they use the same emissions factors (Akagi et al., 2011), thus producing the same relative emissions of different wildfire smoke chemical species. This case study was chosen to compare both of these modeling approaches at a spatial scale on the boundary of where each of these tools are expected to perform well, and where few suitable alternative exists. We found that these two approaches do not present significant differences in absolute model skill; however, we were able to characterize the differences in terms of Negative and PPV of the simulations and link these results to differences in assumed biomass load and burn rate. Because SFIRE is specifically designed for individual fires, uses specified fuel load, and can compute the burnup rate as a function of simulated environmental conditions, the SFIRE modeling framework provides promising improvement opportunities through incorporation of more detailed input data and improved physical models behind the advancing flame front.

We also compared the WRF-Chem simulations with smoke to WRF-Chem simulations in which biomass burning emissions were turned off (NoFire), allowing us to quantify the impact the wildfire smoke had on surface temperature and windspeed. The coupled setup reproduced surface cooling due to smoke shading, and allowed us to investigate some of the implications of widespread cooling, such as regional reductions in windspeed due to a diminution of the regional sea breeze. In addition to impacts smoke can have on solar energy production, this result suggests smoke could have wide-reaching implications for regional stagnation, air quality, and potentially wind energy production, although further study is required to explore these connections.

Data Availability Statement

Datasets for this research are open source and can be found at these in-text data citation references: US EPA, 2016, Schmidt et al., 2013, Levy et al., 2013, Horel et al., 2002. Software used in this research including WRF, WRF Preprocessing System, WRF-Chem, WRF-SFIRE-Chem, and WRF-Chem preprocessing tools are open source and available at in-text citations: Skamarock et al., 2008, Grell et al., 2005, Kochanski et al., 2015, Emmons et al., 2010, Pfister et al., 2011, US EPA, 2016, Guenther et al., 2012, Gettelman et al., 2019, and Wiedenmyer et al., 2011.

Acknowledgments
We would like to thank Dr. Gabriele Pfister for her help troubleshooting our WRF-Chem simulations, and for her suggestions regarding WRF-Chem best practices. This work was funded by Lawrence Livermore National Laboratory LDRD 20-ERD-034, and by the University of California Office of the President (UCOP) through the UCOP Laboratory Fees program under award LFR-20-651032. A partial support for this work came from NASA Grant 80NSSC19K1091, NSF Grant DEB-2039552, Electrical Power Research Institute Grant DKT200194. We would like to acknowledge high-performance computing support from Cheyenne (https://doi.org/10.5065/D6RX99HX) provided by NCAR's Computational- and Information Systems Laboratory, sponsored by the National Science Foundation. This work was performed under the auspices of the U.S. Department of Energy by Lawrence Livermore National Laboratory under Contract DE-AC52-07NA27344.

References

Ainslie, B., So, R., & Chen, J. (2022). Operational evaluation of a wildfire air quality model from a forecaster point of view. *Weather and Forecasting*, *37*(5), 681–698. https://doi.org/10.1175/WAF-D-21-0064.1

Akagi, S. K., Yokelson, R. J., Wiedinmyer, C., Alvarado, M. J., Reid, J. S., Karl, T., et al. (2011). Emission factors for open and domestic biomass burning for use in atmospheric models. *Atmospheric Chemistry and Physics*, *11*(9), 4039–4072. https://doi.org/10.5194/acp-11-4039-2011

Albini, F. A. (1976). Estimating wildfire behavior and effects. Gen. Tech. Rep. INT-GTR-30. Ogden, UT: U.S. Department of Agriculture, Forest Service, Intermountain Forest and Range Experiment Station (Vol. *92*, p. 30). Retrieved from http://www.fs.usda.gov/treesearch/pubs/29574

Andrews, P. L. (2013). Current status and future needs of the BehavePlus fire modeling system. *International Journal of Wildland Fire*, *23*(1), 21–33. https://doi.org/10.1071/WF12167

August Complex Information—InciWeb the Incident Information System. (2020). Retrieved from https://inciweb.nwcg.gov/incident/6983/

Balzarini, A., Pirovano, G., Honzak, L., Žabkar, R., Curci, G., Forkel, R., et al. (2015). WRF-Chem model sensitivity to chemical mechanisms choice in reconstructing aerosol optical properties. *Atmospheric Environment*, *115*, 604–619. https://doi.org/10.1016/j.atmosenv.2014.12.033

Barry, K. R., Hill, T. C. J., Levin, E. J. T., Twohy, C. H., Moore, K. A., Weller, Z. D., et al. (2021). Observations of ice nucleating particles in the free troposphere from Western US wildfires. *Journal of Geophysical Research: Atmospheres*, *126*(3), e2020JD033752. https://doi.org/10.1029/2020JD033752

Bauer, S. E., Menon, S., Koch, D., Bond, T. C., & Tsigaridis, K. (2010). A global modeling study on carbonaceous aerosol microphysical characteristics and radiative effects. *Atmospheric Chemistry and Physics*, *10*(15), 7439–7456. https://doi.org/10.5194/acp-10-7439-2010

Benjamin, S. G., Weygandt, S. S., Brown, J. M., Hu, M., Alexander, C. R., Smirnova, T. G., et al. (2016). A North American hourly assimilation and model forecast cycle: The rapid refresh. *Monthly Weather Review*, *144*(4), 1669–1694. https://doi.org/10.1175/MWR-D-15-0242.1

Campbell, P. C., Bash, J. O., & Spero, T. L. (2019). Updates to the Noah land surface model in WRF-CMAQ to improve simulated meteorology, air quality, and deposition. *Journal of Advances in Modeling Earth Systems*, *11*(1), 231–256. https://doi.org/10.1029/2018MS001422

Carter, T. S., Heald, C. L., Jimenez, J. L., Campuzano-Jost, P., Kondo, Y., Moteki, N., et al. (2020). How emissions uncertainty influences the distribution and radiative impacts of smoke from fires in North America. *Atmospheric Chemistry and Physics*, *20*(4), 2073–2097. https://doi.org/10.5194/acp-20-2073-2020

Chen, D., Liu, Z., Schwartz, C. S., Lin, H.-C., Cetola, J. D., Gu, Y., & Xue, L. (2014). The impact of aerosol optical depth assimilation on aerosol forecasts and radiative effects during a wild fire event over the United States. *Geoscientific Model Development*, *7*(6), 2709–2715. https://doi.org/10.5194/gmd-7-2709-2014

Creek Fire Information - InciWeb the Incident Information System. (2021). Retrieved from https://inciweb.nwcg.gov/incident/7147/

Crutzen, P. J., & Andreae, M. O. (1990). Biomass burning in the tropics: Impact on atmospheric chemistry and biogeochemical cycles. *Science*, *250*(4988), 1669–1678. https://doi.org/10.1126/science.250.4988.1669

Emmons, L. K., Walters, S., Hess, P. G., Lamarque, J.-F., Pfister, G. G., Fillmore, D., et al. (2010). Description and evaluation of the model for Ozone and related chemical Tracers, version 4 (MOZART-4). *Geoscientific Model Development*, *3*(1), 43–67. https://doi.org/10.5194/gmd-3-43-2010

Farguell, A., Mandel, J., Haley, J., Mallia, D. V., Kochanski, A., & Hilburn, K. (2021). Machine learning estimation of fire arrival time from level-2 active fires satellite data. *Remote Sensing*, *13*(11), 2203. https://doi.org/10.3390/rs13112203

Fire Season. (2021). Retrieved from https://www.fire.ca.gov/incidents/2020/

Ford, B., Val Martin, M., Zelasky, S. E., Fischer, E. V., Anenberg, S. C., Heald, C. L., & Pierce, J. R. (2018). Future fire impacts on smoke concentrations, visibility, and health in the contiguous United States. *GeoHealth*, *2*(8), 229–247. https://doi.org/10.1029/2018GH000144

Freitas, S. R., Longo, K. M., Chatfield, R., Latham, D., Silva Dias, M. A. F., Andreae, M. O., et al. (2007). Including the sub-grid scale plume rise of vegetation fires in low resolution atmospheric transport models. *Atmospheric Chemistry and Physics*, *7*(13), 3385–3398. https://doi.org/10.5194/acp-7-3385-2007

Freitas, S. R., Longo, K. M., Trentmann, J., & Latham, D. (2010). Technical Note: Sensitivity of 1-D smoke plume rise models to the inclusion of environmental wind drag. *Atmospheric Chemistry and Physics*, *10*(2), 585–594. https://doi.org/10.5194/acp-10-585-2010

Gan, R. W., Ford, B., Lassman, W., Pfister, G., Vaidyanathan, A., Fischer, E., et al. (2017). Comparison of wildfire smoke estimation methods and associations with cardiopulmonary-related hospital admissions. *GeoHealth*, *1*(3), 122–136. https://doi.org/10.1002/2017GH000073

Gettelman, A., Mills, M. J., Kinnison, D. E., Garcia, R. R., Smith, A. K., Marsh, D. R., et al. (2019). The whole atmosphere community climate model version 6 (WACCM6). *Journal of Geophysical Research: Atmospheres*, *124*(23), 12380–12403. https://doi.org/10.1029/2019JD030943

Grell, G., Freitas, S. R., Stuefer, M., & Fast, J. (2011). Inclusion of biomass burning in WRF-chem: Impact of wildfires on weather forecasts. *Atmospheric Chemistry and Physics*, *11*(11), 5289–5303. https://doi.org/10.5194/acp-11-5289-2011

Grell, G. A., Peckham, S. E., Schmitz, R., McKeen, S. A., Frost, G., Skamarock, W. C., & Eder, B. (2005). Fully coupled "online" chemistry within the WRF model. *Atmospheric Environment*, *39*(37), 6957–6975. https://doi.org/10.1016/j.atmosenv.2005.04.027

Guenther, A. B., Jiang, X., Heald, C. L., Sakulyanontvittaya, T., Duhl, T., Emmons, L. K., & Wang, X. (2012). The model of emissions of gases and aerosols from nature version 2.1 (MEGAN2.1): An extended and updated framework for modeling biogenic emissions. *Geoscientific Model Development*, *5*(6), 1471–1492. https://doi.org/10.5194/gmd-5-1471-2012

Hall, J. V., Zhang, R., Schroeder, W., Huang, C., & Giglio, L. (2019). Validation of GOES-16 ABI and MSG SEVIRI active fire products. *International Journal of Applied Earth Observation and Geoinformation*, *83*, 101928. https://doi.org/10.1016/j.jag.2019.101928

Heikenfeld, M., White, B., Labbouz, L., & Stier, P. (2019). Aerosol effects on deep convection: The propagation of aerosol perturbations through convective cloud microphysics. *Atmospheric Chemistry and Physics*, *19*(4), 2601–2627. https://doi.org/10.5194/acp-19-2601-2019

Herzmann, D. (2020). NWS raw text product. Retrieved from https://mesonet.agron.iastate.edu/wx/afos/p.php?pil=AFDMTR%26e=202009111751

21698996, 2023, 6, Downloaded from https://agupubs.onlinelibrary.wiley.com/doi/10.1029/2022JD037062 by University Of California Irvine Science Library Serials, Wiley Online Library on [29/09/2026]. See the Terms and Conditions (https://onlinelibrary.wiley.com/terms-and-conditions) on Wiley Online Library for rules of use; OA articles are governed by the applicable Creative Commons License

Hodshire, A. L., Akherati, A., Alvarado, M. J., Brown-Steiner, B., Jathar, S. H., Jimenez, J. L., et al. (2019). Aging effects on biomass burning aerosol mass and composition: A critical review of field and laboratory studies. *Environmental Science and Technology*, *53*(17), 10007–10022. https://doi.org/10.1021/acs.est.9b02588

Horel, J., Splitt, M., Dunn, L., Pechmann, J., White, B., Cilberti, C., et al. (2002). Mesowest: Cooperative Mesonets in the Western United States. *Bulletin of the American Meteorological Society*, *83*, 211–216. https://doi.org/10.1175/1520-0477(2002)083%3C0211:MCMITW%3E2.3.CO;2

HRRR-Smoke Graphics. (2020). Retrieved from https://rapidrefresh.noaa.gov/hrrr/HRRRsmoke/

Iacono, M. J., Delamere, J. S., Mlawer, E. J., Shephard, M. W., Clough, S. A., & Collins, W. D. (2008). Radiative forcing by long-lived greenhouse gases: Calculations with the AER radiative transfer models. *Journal of Geophysical Research*, *113*(D13), D13103. https://doi.org/10.1029/2008JD009944

Jen, C. N., Hatch, L. E., Selimovic, V., Yokelson, R. J., Weber, R., Fernandez, A. E., et al. (2019). Speciated and total emission factors of particulate organics from burning Western US wildland fuels and their dependence on combustion efficiency. *Atmospheric Chemistry and Physics*, *19*(2), 1013–1026. https://doi.org/10.5194/acp-19-1013-2019

Jiang, X., Wiedinmyer, C., & Carlton, A. G. (2012). Aerosols from fires: An examination of the effects on Ozone photochemistry in the Western United States. *Environmental Science and Technology*, *46*(21), 11878–11886. https://doi.org/10.1021/es301541k

Karumuri, R. K., Kunchala, R. K., Attada, R., Dasari, H. P., & Hoteit, I. (2022). Seasonal simulations of summer aerosol optical depth over the Arabian Peninsula using WRF-Chem: Validation, climatology, and variability. *International Journal of Climatology*, *42*(5), 2901–2922. https://doi.org/10.1002/joc.7396

Kaufman, Y. J., & Nakajima, T. (1993). Effect of Amazon smoke on cloud microphysics and Albedo-analysis from satellite imagery. *Journal of Applied Meteorology and Climatology*, *32*(4), 729–744. https://doi.org/10.1175/1520-0450(1993)032<0729:EOASOC>2.0.CO;2

Kochanski, A. K., Herron-Thorpe, F., Mallia, D. V., Mandel, J., & Vaughan, J. K. (2021). Integration of a coupled fire-atmosphere model into a regional air quality forecasting system for wildfire events. *Frontiers in Forests and Global Change*, *4*. https://doi.org/10.3389/ffgc.2021.728726

Kochanski, A. K., Jenkins, M. A., Yedinak, K., Mandel, J., Beezley, J., Lamb, B., et al. (2015). Toward an integrated system for fire, smoke and air quality simulations. *International Journal of Wildland Fire*, *25*(5), 534–546. https://doi.org/10.1071/WF14074

Kochanski, A. K., Mallia, D. V., Fearon, M. G., Mandel, J., Souri, A. H., & Brown, T. (2019). Modeling wildfire smoke feedback mechanisms using a coupled fire-atmosphere model with a radiatively active aerosol scheme. *Journal of Geophysical Research: Atmospheres*, *124*(16), 9099–9116. https://doi.org/10.1029/2019JD030558

Lassman, W. (2015). *Blending model output with satellite-based and in-situ observations to produce high-resolution estimates of population exposure to wildfire smoke (Text)*. Colorado State University. Retrieved from https://mountainscholar.org/handle/10217/178887

Lassman, W., Ford, B., Gan, R. W., Pfister, G., Magzamen, S., Fischer, E. V., & Pierce, J. R. (2017). Spatial and temporal estimates of population exposure to wildfire smoke during the Washington state 2012 wildfire season using blended model, satellite, and in situ data. *GeoHealth*, *1*(3), 106–121. https://doi.org/10.1002/2017GH000049

Levy, R. C., Mattoo, S., Munchak, L. A., Remer, L. A., Sayer, A. M., Patadia, F., & Hsu, N. C. (2013). The Collection 6 MODIS aerosol products over land and ocean. *Atmospheric Measurement Techniques*, *6*(11), 2989–3034. https://doi.org/10.5194/amt-6-2989-2013

Lindaas, J., Pollack, I. B., Garofalo, L. A., Pothier, M. A., Farmer, D. K., Kreidenweis, S. M., et al. (2021). Emissions of reactive nitrogen from Western U.S. Wildfires during summer 2018. *Journal of Geophysical Research: Atmospheres*, *126*(2), e2020JD032657. https://doi.org/10.1029/2020JD032657

Liu, Y., Goodrick, S., & Heilman, W. (2014). Wildland fire emissions, carbon, and climate: Wildfire–climate interactions. *Forest Ecology and Management*, *317*, 80–96. https://doi.org/10.1016/j.foreco.2013.02.020

Lutes, D. C. (2013). Predicted fuel consumption in the burnup model: Sensitivity to four user inputs. Res. Note RMRS-RN-51WWW. U.S. Department of Agriculture, Forest Service, Rocky Mountain Research Station (Vol. *11*, p. 51). https://doi.org/10.2737/RMRS-RN-51

Mallia, D. V., Kochanski, A. K., Urbanski, S. P., & Lin, J. C. (2018). Optimizing smoke and plume rise modeling approaches at local scales. *Atmosphere*, *9*(5), 166. https://doi.org/10.3390/atmos9050166

Mellor, G. L., & Yamada, T. (1982). Development of a turbulence closure model for geophysical fluid problems. *Reviews of Geophysics*, *20*(4), 851–875. https://doi.org/10.1029/RG020i004p00851

Mu, M., Randerson, J. T., van der Werf, G. R., Giglio, L., Kasibhatla, P., Morton, D., et al. (2011). Daily and 3-hourly variability in global fire emissions and consequences for atmospheric model predictions of carbon monoxide. *Journal of Geophysical Research*, *116*(D24). https://doi.org/10.1029/2011JD016245

NCEP GFS 0.25 Degree Global Forecast Grids Historical Archive. (2015). *NCEP GFS 0.25 degree global forecast grids historical archive*. Research Data Archive at the National Center for Atmospheric Research, Computational and Information Systems Laboratory. https://doi.org/10.5065/D65D8PWK

Nonsingular implementation of the Mellor-Yamada level 2.5 scheme in the NCEP Meso model. (2001). Nonsingular implementation of the Mellor-Yamada level 2.5 scheme in the NCEP Meso model. Retrieved from https://repository.library.noaa.gov/view/noaa/11409

O'Dell, K., Bilsback, K., Ford, B., Martenies, S. E., Magzamen, S., Fischer, E. V., & Pierce, J. R. (2021). Estimated mortality and morbidity attributable to smoke plumes in the United States: Not just a Western US problem. *GeoHealth*, *5*(9), e2021GH000457. https://doi.org/10.1029/2021GH000457

O'Dell, K., Ford, B., Fischer, E. V., & Pierce, J. R. (2019). Contribution of wildland-fire smoke to US PM2.5 and its influence on recent trends. *Environmental Science and Technology*, *53*(4), 1797–1804. https://doi.org/10.1021/acs.est.8b05430

O'Dell, K., Hornbrook, R. S., Permar, W., Levin, E. J. T., Garofalo, L. A., Apel, E. C., et al. (2020). Hazardous air pollutants in fresh and aged Western US wildfire smoke and implications for long-term exposure. *Environmental Science and Technology*, *54*(19), 11838–11847. https://doi.org/10.1021/acs.est.0c04497

Pavlovic, R., Chen, J., Anderson, K., Moran, M. D., Beaulieu, P.-A., Davignon, D., & Cousineau, S. (2016). The FireWork air quality forecast system with near-real-time biomass burning emissions: Recent developments and evaluation of performance for the 2015 North American wildfire season. *Journal of the Air and Waste Management Association*, *66*(9), 819–841. https://doi.org/10.1080/10962247.2016.1158214

Pfister, G. G., Avise, J., Wiedinmyer, C., Edwards, D. P., Emmons, L. K., Diskin, G. D., et al. (2011). CO source contribution analysis for California during ARCTAS-CARB. *Atmospheric Chemistry and Physics*, *11*(15), 7515–7532. https://doi.org/10.5194/acp-11-7515-2011

Ramnarine, E., Kodros, J. K., Hodshire, A. L., Lonsdale, C. R., Alvarado, M. J., & Pierce, J. R. (2019). Effects of near-source coagulation of biomass burning aerosols on global predictions of aerosol size distributions and implications for aerosol radiative effects. *Atmospheric Chemistry and Physics*, *19*(9), 6561–6577. https://doi.org/10.5194/acp-19-6561-2019

Reid, C. E., Brauer, M., Johnston, F. H., Jerrett, M., Balmes, J. R., & Elliott, C. T. (2016). Critical review of health impacts of wildfire smoke exposure. *Environmental Health Perspectives*, *124*(9), 1334–1343. https://doi.org/10.1289/ehp.1409277

Reinhardt, E. (2003). *Using FOFEM 5.0 to estimate tree mortality, fuel consumption, smoke production and soil heating from wildland fire*. American Meteorological Society. Retrieved from https://www.frames.gov/catalog/819

21698996, 2023, 6, Downloaded from https://agupubs.onlinelibrary.wiley.com/doi/10.1029/2022JD037062 by University Of California Irvine Science Library Serials, Wiley Online Library on [29/09/2026]. See the Terms and Conditions (https://onlinelibrary.wiley.com/terms-and-conditions) on Wiley Online Library for rules of use; OA articles are governed by the applicable Creative Commons License

Robock, A. (1991). Surface cooling due to forest fire smoke. *Journal of Geophysical Research*, *96*(D11), 20869–20878. https://doi.org/10.1029/91JD02043

Schmidt, C. C., Hoffman, J., Prins, E., & Lindstrom, S. (2013). GOES-R advanced baseline imager (ABI) algorithm theoretical basis document for fire/hot spot characterization.

Schreier, S. F., Richter, A., Kaiser, J. W., & Burrows, J. P. (2014). The empirical relationship between satellite-derived tropospheric NO_2 and fire radiative power and possible implications for fire emission rates of NO_x. *Atmospheric Chemistry and Physics*, *14*(5), 2447–2466. https://doi.org/10.5194/acp-14-2447-2014

Siméon, A., Waquet, F., Péré, J.-C., Ducos, F., Thieuleux, F., Peers, F., et al. (2021). Combining POLDER-3 satellite observations and WRF-Chem numerical simulations to derive biomass burning aerosol properties over the southeast Atlantic region. *Atmospheric Chemistry and Physics*, *21*(23), 17775–17805. https://doi.org/10.5194/acp-21-17775-2021

Skamarock, W., Klemp, J., Dudhia, J., Gill, D., Barker, D., Wang, W., et al. (2008). *A description of the advanced research WRF version 3 [Application/pdf]* (p. 1002 KB). UCAR/NCAR. https://doi.org/10.5065/D68S4MVH

Stone, R. S., Augustine, J. A., Dutton, E. G., O'Neill, N. T., & Saha, A. (2011). Empirical determinations of the longwave and shortwave radiative forcing efficiencies of wildfire smoke. *Journal of Geophysical Research*, *116*(D12), D12207. https://doi.org/10.1029/2010JD015471

Thompson, G., Rasmussen, R. M., & Manning, K. (2004). Explicit forecasts of winter precipitation using an improved bulk microphysics scheme. Part I: Description and sensitivity analysis. *Monthly Weather Review*, *132*(2), 519–542. https://doi.org/10.1175/1520-0493(2004)132<0519:EFOWPU>2.0.CO;2

US EPA, O. (2014). Air data: Air quality data collected at outdoor monitors across the US [collections and lists]. Retrieved from https://www.epa.gov/outdoor-air-quality-data

US EPA, O. (2016). 2014 national emissions inventory (NEI) data [other policies and guidance]. Retrieved from https://www.epa.gov/air-emissions-inventories/2014-national-emissions-inventory-nei-data

Val Martin, M., Heald, C. L., Ford, B., Prenni, A. J., & Wiedinmyer, C. (2013). A decadal satellite analysis of the origins and impacts of smoke in Colorado. *Atmospheric Chemistry and Physics*, *13*(15), 7429–7439. https://doi.org/10.5194/acp-13-7429-2013

Westerling, A. L., Hidalgo, H. G., Cayan, D. R., & Swetnam, T. W. (2006). Warming and earlier spring increase Western U.S. Forest wildfire activity. *Science*, *313*(5789), 940–943. https://doi.org/10.1126/science.1128834

Wiedinmyer, C., Akagi, S. K., Yokelson, R. J., Emmons, L. K., Al-Saadi, J. A., Orlando, J. J., & Soja, A. J. (2011). The fire INventory from NCAR (FINN): A high resolution global model to estimate the emissions from open burning. *Geoscientific Model Development*, *4*(3), 625–641. https://doi.org/10.5194/gmd-4-625-2011

Wiedinmyer, C., Quayle, B., Geron, C., Belote, A., McKenzie, D., Zhang, X., et al. (2006). Estimating emissions from fires in North America for air quality modeling. *Atmospheric Environment*, *40*(19), 3419–3432. https://doi.org/10.1016/j.atmosenv.2006.02.010

Wiggins, E. B., Soja, A. J., Gargulinski, E., Halliday, H. S., Pierce, R. B., Schmidt, C. C., et al. (2020). High temporal resolution satellite observations of fire radiative power reveal link between fire behavior and aerosol and gas emissions. *Geophysical Research Letters*, *47*(23), e2020GL090707. https://doi.org/10.1029/2020GL090707

Yang, E.-S., Christopher, S. A., Kondragunta, S., & Zhang, X. (2011). Use of hourly Geostationary Operational Environmental Satellite (GOES) fire emissions in a Community Multiscale Air Quality (CMAQ) model for improving surface particulate matter predictions. *Journal of Geophysical Research*, *116*(D4), D04303. https://doi.org/10.1029/2010JD014482

Yao, J., Brauer, M., Wei, J., McGrail, K. M., Johnston, F. H., & Henderson, S. B. (2020). Sub-daily exposure to fine particulate matter and ambulance dispatches during wildfire seasons: A case-Crossover study in British Columbia, Canada. *Environmental Health Perspectives*, *128*(6), 067006. https://doi.org/10.1289/EHP5792

21698996, 2023, 6, Downloaded from https://agupubs.onlinelibrary.wiley.com/doi/10.1029/2022JD037062 by University Of California Irvine Science Library Serials, Wiley Online Library on [29/09/2026]. See the Terms and Conditions (https://onlinelibrary.wiley.com/terms-and-conditions) on Wiley Online Library for rules of use; OA articles are governed by the applicable Creative Commons License